Electrochemical Ammonia Production Using Pyrolyzed Cobalt Phthalocyanine

A Thesis submitted to
Indian Institute of Science Education and Research (IISER), Pune
In partial fulfilment of the requirements for the MSc Degree Programme

By

Abhishek A P

(Registration No. 20226203)

Indian Institute of Science Education and Research (IISER), Pune
Dr. Homi Bhabha Road,
Pashan, Pune-411008, India

April, 2024

Supervisor:

Prof. Muhammed Musthafa O T

(Department of Chemistry, IISER, Pune)

CERTIFICATE

This is to certify that this dissertation entitled **"Electrochemical Ammonia Production Using Pyrolyzed Cobalt Phthalocyanine"** towards the partial fulfilment of the MSc Chemistry program at the Indian Institute of Science Education and Research, Pune represents study/work carried out by **Abhishek A P (Reg No. 20226203)** at Indian Institute of Science Education and Research (IISER), Pune under the supervision of **"Prof. Muhammed Musthafa O T, Department of Chemistry, IISER Pune** during the academic year 2023-2024.

Date: 16/04/2024

Place: Pune

Prof. Muhammed Musthafa O T

Department of Chemistry

Indian Institute of Science Education and Research, Pune

India 411008

DECLARATION

I hereby declare that the research work presented in the report entitled "**Electrochemical Ammonia Production Using Pyrolyzed Cobalt Phthalocyanine**" has been carried out by me at the **Department of Chemistry, Indian Institute of Science Education and Research, Pune** under the supervision of **Prof. Muhammed Musthafa O T** and the same has not been submitted elsewhere for any degree.

Date: 12/04/2024

Place: Pune

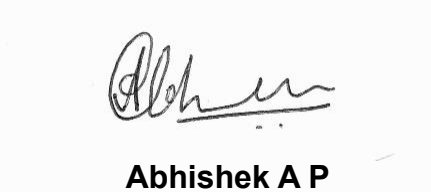

Abhishek A P

(Registration No. 20226203)

Prof. Muhammed Musthafa O T

Department of Chemistry

Indian Institute of Science Education and Research, Pune

India 411008

ACKNOWLEDGEMENTS

The completion of this thesis would not have been possible without the unwavering support of my family, teachers, and friends. I have no words to express how grateful I am for my parents' unending love, support, and care throughout my life. First and foremost, I would like to express my sincere gratitude to my supervisor, **Professor Muhammed Musthafa**, for his invaluable guidance and encouragement throughout this process. His expertise and insightful feedback were essential in shaping this research and carrying it forward. I thank my additional TAC expert member **Prof. Partha Hazra** (IISER Pune), for his valuable suggestions during my presentations and report submissions. I am also deeply grateful to my mentor, Rahul Mahadeo Mendhe, whose continuous support and mentorship provided me with the confidence and direction I needed to navigate this academic journey.

Furthermore, I extend my heartfelt thanks to my parents for their unwavering love and belief in me. Their constant encouragement and unwavering support served as a source of immense strength throughout my studies. I thank Ritwik Mondal and Sanchayita Mukhopadhyay for teaching & helping me with various electrochemical and material characterization. I thank Anweshi Dewan and Hitesh Kumar for teaching me electrochemistry basics and supporting me throughout my initial phase. I thank my best friend and my lab mate Akshay H for supporting me throughout my thesis. I appreciate all other lab members, especially Shifali Dutt & Muskan Parmar for continuous mentoring by teaching me various analytical skills. I thank Bhoj Kumar Nayak and Hemanga Pradhan for helping me with conducting experiments. I would like to thank my batchmates and seniors for supporting me throughout.

CONTENTS

ABSTRACT……...10

1. INTRODUCTION…….....11

1.1. Electrochemical Methods

1.1.1. Electrochemical Reduction

1.1.2. Electrochemical Oxidation

2. MATERIALS & METHODS…….....15

2.1. Chemicals

2.2. Material Synthesis

2.3. Experimental Section

2.3.1. Electrochemical Characterization

2.3.2. Material Characterization

3. RESULTS & DISCUSSION…….....22

4. CONCLUSION…….....43

REFERENCES…….....44

LIST OF FIGURES

Label	Title	Page
Figure 2.1	Steps involved in the pyrolysis of materials	16
Figure 2.2	Schematic representation of a cyclic Voltammogram	17
Figure 3.1	Thermogravimetric analysis of pristine CoPc and its composites	22
Figure 3.2	(a) X-ray Diffraction of pristine CoPc, CNT and pyrolyzed composites (b) UV-Vis spectrum of pristine CoPc, and composites before after pyrolysis	23
Figure 3.3	(a) FTIR spectra of pristine CoPc, and composites before and after pyrolysis (b) Raman spectra of pristine CoPc, and composites before and after pyrolysis	24
Figure 3.4	TEM and EDX of (a) pristine CoPc (b) CoPc after pyrolysis (c) CoPc CNT (50%) after pyrolysis (d) CoPc CNT (60%) after pyrolysis and (e) CoPc CNT (70%) after pyrolysis	25
Figure 3.5	Linear sweep voltammetry of (a) pristine CoPc, CoPc after pyrolysis and CoPc CNT (60%) after pyrolysis Linear sweep voltammetry of (b) CoPc CNT (50%) before and after pyrolysis, CoPc CNT (60%) before and after pyrolysis, and CoPc CNT (70%) before and after pyrolysis	26
Figure 3.6	(a) Tafel plots of pyrolyzed CoPc composites (b) Nyquist plots of pyrolyzed CoPc composites	27
Figure 3.7	Photograph of two compartment cell used for ammonia synthesis	28
Figure 3.8	(a) UV-Vis spectra of nitrate at different concentrations (b) the calibration curve for nitrate.	29
Figure 3.9	(a) ^{1}H NMR spectra of ammonium ion at different concentrations (b) calibration curve for ammonium ion	30

Figure 3.10	(a) UV-Vis spectra of ammonium ion at different concentrations (b) Calibration curve for ammonium ion at different concentrations (c) Photographs of ammonia solutions at different concentrations with indophenol blue.	31
Figure 3.11	(a) UV-Vis spectra of nitrite at different concentrations (b) Calibration curve of nitrite at different concentrations (c) Photographs of nitrite solutions at different concentrations with naphthyl ethylenediamine dihydrochloride, and p-amino-benzene sulfonamide	32
Figure 3.12	In-situ electrochemical mass spectrometry analysis during nitrate reduction showing the presence of hydrogen evolution	33
Figure 3.13	(a) Chronoamperometry traces at different potentials for 2 h (b) ^{1}H NMR spectra demonstrating ammonium ion formation (c) UV-Vis spectra of nitrate before and after reaction (d) Yield rate and Faradaic efficiency at different potentials	34
Figure 3.14	(a) UV-Vis spectra of nitrate before and after reaction for 20 h at different potentials (b) ^{1}H NMR of ammonium ion in the product solution at different potentials (c) Quantification of ammonium and nitrate in the solution after the reaction	35
Figure 3.15	Contact angle measurements of (a) MWCNT (b) pristine CoPc (c) CoPc after pyrolysis (d) CoPc CNT (50%) after pyrolysis (e) CoPc CNT (60%) after pyrolysis (f) CoPc CNT (70%) after pyrolysis.	36
Figure 3.16	BET Nitrogen adsorption desorption isotherm of pristine CoPc, CNT and composites after pyrolysis	37
Figure 3.17	Cyclic voltammograms of (a) pristine CoPc (b) CoPc after pyrolysis (c) CoPc CNT (50%) after pyrolysis (d) CoPc CNT (60%) after pyrolysis (e) CoPc CNT (70%) after pyrolysis (f) Electrochemical active surface area (ECSA).	39

Figure 3.18	Schematic representation of ammonia synthesis during electroreduction of nitrate	40
Figure 3.19	Schematic representation of the catalytic cycle describing electrochemical nitrate reduction on pyrolyzed cobalt catalyst	42

LIST OF TABLES

Label	Title	Page
Table 1	Abbreviations and their full forms	14
Table 2	Electrodes and their functions	17
Table 3	Instrumentation details.	19
Table 4	I_D/I_G ratio extracted from the Raman spectra.	24
Table 5	Surface areas of CoPc, CNT and the composites before and after pyrolysis	38

ABSTRACT

Water pollution has become a significant global concern in recent years. Industrial and agricultural effluents discharged directly pose a threat to the ecological system, necessitating treatment and decontamination before release. Ammonia holds great promise in the future energy industry owing to its high energy density, carbon-free hydrogen storage capabilities, and emission cleanliness. Combining ammonia synthesis with nitrate removal presents a sustainable and economically viable solution for treating nitrate-contaminated water. However, existing electrodes may encounter challenges in achieving satisfactory selectivity and Faradaic efficiency due to the complex eight-electron transfer pathway involved in nitrate reduction to ammonia and competition with hydrogen evolution reactions. Therefore, there is a need to develop high-performance electrocatalysts capable of selectively reducing nitrate. So here we developed an electrode based on pyrolyzed cobalt phthalocyanine for the nitrate reduction to ammonia. Non-precious electrocatalysts for the nitrate reduction were synthesized using cobalt phthalocyanine (CoPc) and functionalized multi-walled carbon nanotubes (CNTs). These electrocatalysts undergo thermal treatment within a temperature range of 500 to 700°C. The impact of pyrolysis temperature on the electrocatalytic activity for nitrate reduction was analyzed through various techniques. The pyrolyzed catalyst results in a notable ammonia yield of nearly 0.26 mg h^{-1} cm^{-2} with a Faradaic efficiency of nearly 53 % at -0.9 V vs Ag/AgCl/Cl^-. The improved activity after pyrolysis is attributed to the well dispersion of Co based oxides and Co-Nx sites on the carbon support, which lead to notably higher yield rate, Faradaic efficiency, conversion and stability.

Chapter 1

INTRODUCTION

Temperature rise is one of the major concerns that is faced by living beings, this process is known as global warming. That leads to the long-term rise in the average temperature of the Earth driven mostly by human activities that emit greenhouse gases into the atmosphere [1]. These gases act like a blanket, trapping heat and disrupting the Earth's regular temperature patterns [2]. Global warming's consequences are far-reaching and already felt around the world, making it a serious subject that requires our attention. Our reliance on fossil fuels such as coal, oil, and natural gas has far-reaching consequences [3]. Burning these energy sources causes the atmosphere to fill with greenhouse gases, mainly carbon dioxide [4]. This phenomenon will affect weather patterns and melting glaciers that cause rising sea levels [5]. The impacts are extensive, affecting not just human health and infrastructure but also ecosystems and agriculture [6,7]. Scientists have identified that fossil fuel usage is the primary cause of global warming, making the move to cleaner energy sources critical for preserving the world for future generations [8,9].

Hydrogen fuel is a promising alternative to fossil fuels in the future due to Its clean burning nature is its biggest benefit [10]. When utilized in a fuel cell, it emits solely water vapor and leaves no hazardous pollutants behind [11]. Therefore, it is perfect for preventing climate change. The most common element on Earth is hydrogen and also which can be produced through sustainable energy sources like solar [12] and wind power [13]. However, there are still challenges to be addressed. Hydrogen gas has significant drawbacks when it comes to storage and use, despite its potential as a clean fuel. The greatest difficulty is its poor energy density per volume [14,15]. This implies that storing enough hydrogen for practical uses requires a huge amount of area, which makes it inconvenient for cars and challenging for large-scale storage. Current techniques, such as compressed gas tanks, require high pressure, which adds weight and complexity [16]. Even liquefaction, which increases density, requires extremely low temperatures and specialized equipment, making it both costly and energy-intensive. Safety problems are also raised by the fact that hydrogen is extremely combustible and can leak through some materials [17]. These restrictions

prevent hydrogen technology from being widely used. Large-scale manufacturing and effective storage methods are being actively investigated to make hydrogen a more inexpensive and realistic clean energy solution [18]. Ammonia, on the other hand, is easier to liquefy and has a higher energy density per volume than liquid hydrogen and this makes long-distance transportation more feasible [19]. Furthermore, the breakdown of ammonia, known as cracking, produces hydrogen gas, which can be used in fuel cells and other uses [20]. This process also produces nitrogen, a harmless gas that makes up the majority of the Earth's atmosphere. All things considered, ammonia fills the gap between hydrogen's potential for clean energy and the practical difficulties associated with its storage and transportation.

Water pollution is also a serious problem faced by this generation and nitrate pollution is one among them [21]. Common fertilizer ingredient nitrate can contaminate water when it seeps into the ground or runs off into surface waters in excess. This contamination is generally caused by agricultural operations, such as residual fertilizer or manure leaching from fields [22]. When these nitrates are found in large enough concentrations in drinking water, they can alter ecosystems by causing excessive plant growth in bodies of water. For humans also 33 to 250 mg of nitrite per kg of body weight consumption is fatal [23]. The most serious health danger linked to nitrate is methemoglobinemia, or "blue baby syndrome," a disorder that develops when the body breaks down nitrates into nitrites, particularly in the digestive tract [24]. Nitrites then interfere with hemoglobin’s ability to transport oxygen in the blood, changing its structure and rendering it ineffective in binding oxygen. As a result, there is not enough oxygen getting to the tissues, which causes symptoms including weariness, headaches, cyanosis, and shortness of breath [25]. Because of their immature nitrite-degrading enzyme system, newborns under six months old are especially susceptible to the potentially lethal effects of severe methemoglobinemia.

Cobalt phthalocyanine is a versatile compound that has emerged to become a key player in the field of electrochemistry, providing with wide variety of applications that have revolutionized the development of many fields like electrochemistry and material sciences [26]. Cobalt phthalocyanine (CoPc) has a deep blue colour. It is a planar molecule with an N_4 macrocyclic ring and a metal ion embodied at the center of the plane. This structural advantage is the main reason for the emergence of metal phthalocyanine in the above-mentioned fields. Cobalt phthalocyanine's unique

molecular structure and electron-rich nature make it an ideal candidate for a variety of electrochemical processes [27]. Its immense applications are spread across plenty of fields including energy storage, catalysis, electrocatalysis, sensors, and photoelectrochemical devices [28]. In this research, cobalt phthalocyanine composite was made with carbon nanotubes [29] and evaluated the catalytic activity for nitrate reduction. The presence of carbon nanotubes increases the stability by acting as an anchor for the catalyst, and it can provide high surface area, enhance the exposure of active sites, and thereby improve the electrochemical properties like hydrogen evolution [30] and oxygen reduction [31], and finally increases the electrical conductivity. Cobalt phthalocyanine and its different composites were pyrolyzed at 700 degrees Celsius [32]. Pyrolyzing involves heating these compositions to high temperatures in the absence of oxygen (inert atmosphere). Heating a compound at high temperature changes its physical as well as chemical properties. Here we have investigated the effect of pyrolysis towards the nitrate reduction and ammonia synthesis and has been found that after pyrolysis there is an enhancement of the catalytic activity. This enhancement in activity was attributed to cobalt oxide formation during pyrolysis at 700℃. The changes in the activity of these materials towards the reduction and oxidation of hazardous nitrate [33] and hydrazine [34] respectively.

1.1 Electrochemical methods

1.1.1 Electrochemical Reduction

Electrochemical reduction is a fundamental electrochemical reaction whereby a chemical species gains electrons at an electrode interface [35]. Electrons are supplied by an external electrical circuit and the electrode at which reduction occurs is called cathode. Electrochemical reduction has a vital role in many fields such as energy storage, corrosion science, and electrochemical synthesis. This property of a species to undergo reduction and gain electrons is measured by its reduction potential. Reduced products are formed when reduction takes place and the electrode potential is greater than the species' standard reduction potential. The electrode material, surface area, species concentration in solution, and applied potential are some of the variables that affect the rate and degree of reduction/oxidation reaction. Advances in energy storage, materials synthesis, and environmental protection are made possible

by the diverse and vital process of electrochemical reduction, which finds extensive applications in industry, research, and technology development.

1.1.2 Electrochemical Oxidation

Electrochemical oxidation is a fundamental process that occurs at the interface of an electrode and a solution containing the substrate to be oxidized. New chemical species are formed as a result of the substance's electrons being transferred to the electrode. An electrical potential given to the external circuit causes an electron flow, which in turn drives this oxidation reaction [35]. Electrons are liberated and the substance being oxidized loses electrons at the anode, this will lead to the creation of ions or compounds with higher oxidation states. Electrochemical oxidation has applications in wide range of sectors, including energy storage, synthesis of valuable compounds, and restoration of the environment. Electrochemical oxidation techniques, such as electrocoagulation and electrooxidation, are employed in water treatment to eliminate heavy metals, break down organic contaminants, and sterilize water. These methods are very useful for treating industrial wastewater and provide an eco-friendly substitute for conventional approaches. Furthermore, oxidation-reduction events at the electrodes of energy storage devices like batteries and fuel cells, which allow the storage and transfer of electrical energy, depend heavily on electrochemical oxidation.

Table 1: Abbreviations and their full forms.

Abbreviation	Full form
CoPc	Cobalt phthalocyanine
MWCNT	Multiwalled Carbon Nanotubes
LSV	Linear Sweep Voltammetry
CV	Cyclic Voltammetry
NMR	Nuclear Magnetic Resonance
GDL electrode	Gas Diffusion Layer
EIS	Electrochemical Impedance Spectroscopy
TGA	Thermal Gravimetric Analysis
TEM	Transmission Electron Microscopy
FTIR	Fourier Transform Infrared spectroscopy
ECSA	Electrochemical surface area

Chapter 2

Materials and methods

This section discusses the synthesis procedure, electrochemical, and physiochemical characterizations.

2.1 Material required

Cobalt phthalocyanine (Sigma Aldrich, 97%), Multiwalled Carbon nanotubes (Sigma Aldrich), Isopropyl alcohol (Rankem, 99%), Perchloric acid (Fischer Chemicals, 70%), Sodium nitrate (Rankem, 99.5%), Sulfuric acid (Rankem, 96%), Nafion resin (Sigma), Nitric acid (Rankem), sodium nitrate (Rankem), Perchloric acid (Fisher), Dimethylsulfoxide (SDFCL), Dimethylsulfoxide-d6 (Sigma), Potassium bromide (SD fine), Maleic acid (Loba chemicals), Phenol crystal (Loba), ammonium chloride (Alfa aesar), soidum nitrite (Sigma), sodium hydroxide (Rankem), trisodium citrate (Rankem), naphthyl ethylenediamine dihydrochloride (Himedia), P-aminobenzene sulfonamide (Sigma), hydrochloric acid (Rankem), sulfamic acid (Sigma)., sodium nitroprusside (Himedia).

2.2 Synthesis of pyrolyzed cobalt phthalocyanine and multiwalled carbon nanotube composites

We synthesized composites using different weight percentages of commercial Cobalt phthalocyanine and Multiwalled Carbon nanotubes. We performed pyrolysis on these composites and pristine CoPc. As different compositions, we used 50, 60, and 70 weight percentages of MWCNT [36]. These materials were mixed by physical means with the help of mortar and pestle [35]. IPA was added to mix these solid compounds properly and grinded it and waited for it to dry. This procedure was repeated 7 to 8 times and took around 3 hours. These composite materials were subjected to pyrolysis at 700℃ for 1 hour in the Ar atmosphere with a heating rate of 5℃/min. After pyrolysis, the products were weighed and stored inside a desiccator. Pyrolyzed materials are

further used for material characterization. Commercial carbon nanotubes are hydrophobic; therefore, the CNT was treated with acid to make it hydrophilic.

For acid treatment, a solution was made of 3:1 ratio 10 M H_2SO_4 and 10 M HNO_3 respectively. 250 mg of MWCNT was added to 250 ml of the above-mentioned solution, and this was subjected to oil bath reflux for 5 hr at 120℃. The product was diluted with water and decanted using centrifugation. After the solution reached pH = 5, the product was separated and dried overnight at 80℃ [37].

Figure 2.1: Steps involved in the pyrolysis of materials.

2.3 Experimental section

2.3.1 Electrochemical Characterization

Electrochemical methods were carried out in a three-electrode setup, with glassy carbon as the working electrode, Pt disc as the counter electrode, and Ag/AgCl/Cl^- as the reference electrode. Material coated glassy carbon was used as working electrode, and the drop casting ink was prepared by dispersing 2 mg of material to the solution of 1 ml of IPA and 20 µl of Nafion solution.

Cyclic voltammetry (CV), linear sweep voltammetry (LSV), chronoamperometry, and electrochemical impedance spectroscopy (EIS) were carried out in a three-electrode setup. In this system, the current is measured between the working electrode and the counter electrode but the potential obtained corresponds to the reference electrode. For initial electrochemical characterizations like cyclic voltammetry, EIS, and LSV the glassy carbon was used as the working electrode, and product analysis was carried out by long-time chronoamperometry for 20 hrs using a GDL electrode. Glassy carbon was cleaned after every reaction using standard methods like water polishing, alumina

powder polishing, and acid cleaning. Acid cleaning was performed in 0.5 M H_2SO_4 solution with Pt disc as counter electrode and Ag/AgCl/Cl^- as a reference electrode in the potential range of +1.1 V to -0.2 V.

Table 2: Electrodes and their functions.

Electrode	Function
Glassy carbon	Working electrode
Ag/AgCl electrode	Reference electrode
Pt disc	Counter electrode
GDL electrode	Working electrode
Pt mesh	Counter electrode
Hg/HgO electrode	Reference electrode

a) Cyclic voltammetry

Cyclic voltammetry is a popular electrochemical method used to study the oxidative and reductive properties of a chemical species [35]. This involves transfer of electrons and with respect to this, we get the current, profile obtained is called cyclic voltammogram. The cyclic voltammogram profile consists of potential on the x-axis and current on the y-axis. In cyclic voltammetry, the sweep in potential between two vertex initial potential (E_1) and final potential (E_2) and corresponding current will be measured.

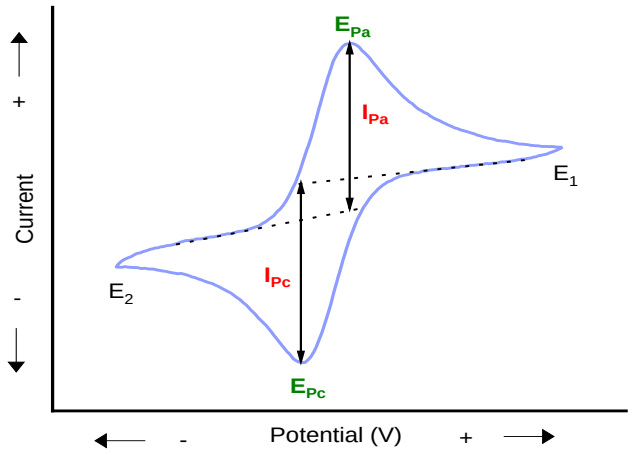

Figure 2.2: Schematic representation of a cyclic Voltammogram.

b) Chronoamperometry

Chronoamperometry is a strong electroanalytical technique for investigating electrochemical processes and characterizing electrode responses. Chronoamperometry measures the current as a function of time by applying a constant voltage to an electrochemical cell [35]. The fundamental idea of chronoamperometry stems from Faraday's law of electrolysis, which asserts that the charge transmitted through the cell is directly proportionate to the amount of material oxidizing or reducing at an electrode. Chronoamperometry is a useful technique for determining the concentration of electroactive species in solution as well as response rates and mechanisms by monitoring the current over time under well controlled experimental conditions. This technology has numerous uses, including the development of electrochemical sensors, corrosion investigations, and the investigation of electrocatalytic processes.

c) Electrochemical Impedance Spectroscopy (EIS)

Electrochemical impedance spectroscopy (EIS) is an experimental AC technique that involves measuring the complex impedance Z of an electrochemical system in steady state or equilibrium. The measurement of the impedance is based on the frequency f (Hertz, or cycles per second) or the angular frequency $\omega=2\pi f$ ($rads^{-1}$) of a small amplitude sinusoidal disturbance that is imposed. At room temperature, the applied potential's amplitude typically falls between ±5 and ±25 mV. The reason "spectroscopy" exists is because frequency is used as a variable [35]. There is a discernible phase angle and time lag between the response signal and the time-dependent excitation because distinct processes at the electrode's surface absorb electric energy at distinct frequencies.

2.3.2 Material Characterization

Materials characterization is a crucial process that involves utilizing a range of analytical instruments, techniques, and methodologies to investigate, measure, and determine a material's chemical, microstructure, and physical properties. TGA, XRD, UV-Vis spectroscopy, FTIR spectroscopy, Raman spectroscopy, and TEM were performed and the instruments used for each method are mentioned in Table 3.

Table 3: Instrumentation details.

Instrument	Company
Electrochemical studies	BioLogic VMP-300
X-ray diffractometer	Bruker D8 Advanced xray diffractometer
Thermogravimetric analyzer	Perkin Elmer STA 6000
UV-Vis spectrometer	Shimadzu UV-1900
FTIR spectrometer	Alpha T spectrometer
Raman spectrometer	ProRaman-L
Transmission electron microscope	JEM-2200FS
NMR spectrometer	Brooker 400 MHz
Mass spectrometer	Hiden Analytical

a) Thermogravimetric analysis (TGA)

Thermal gravimetric analysis (TGA) is a technique commonly used to investigate the thermal degradation of materials [45]. TGA is useful for determining the thermal stability and breakdown characteristics of cobalt phthalocyanine. The temperature at which cobalt phthalocyanine begins to degrade and the degree of degradation can be evaluated by heating the sample under controlled conditions and measuring weight loss as a function of temperature [46]. Understanding its thermal properties is critical since it can be used in a range of applications, including the development of materials for electronics, catalysis, and other fields that require cobalt phthalocyanine.

b) X-ray diffraction

X-ray diffraction is a technique for studying the crystal structure of materials. By using diffraction studies, this technique can be applied since cobalt phthalocyanine has a crystal structure [39]. The interaction of the X-rays with the crystal lattice causes them to diffract and produce a diffraction pattern on a detector. By analysing the angles and intensities of diffracted X-rays, the atomic configuration of the cobalt phthalocyanine crystal can be determined. This information is critical for comprehending its structural features, including bond lengths, angles, and symmetry.

c) UV-Vis Spectroscopy

UV-visible spectroscopy is a technique for determining a chemical compound's light absorbance in both the ultraviolet (UV) and visible range of an electromagnetic spectrum [41]. This method allows us to ascertain cobalt phthalocyanine's concentration and electronic structure [42]. This was done using a UV 1900 spectrometer in the 800-300 nm region, with DMSO as the solvent. Solutions were made with 2 mg of all materials in 0.5 ml DMSO [43].

d) FTIR Spectroscopy

Infrared spectroscopy for cobalt phthalocyanine involves measuring the absorption of infrared radiation by the compound. This method aids in structural analysis and identifies functional groups that are present in cobalt phthalocyanine by providing information on the vibrational modes of the molecule [44]. By analyzing the specific IR absorption peaks, researchers can gain insights into the compound's composition, chemical bonds, and coordination environment around the cobalt atom. This was conducted in Alpha T spectrometer in KBr pellet mode in a range of 650 to 2500 cm^{-1}. With the help of this technique, we can compare the changes in bond vibrations. KBr pellet was prepared by grinding dried KBr using mortar pestle and added to pellet case for applying pressure.

e) Transmission Electron Microscopy

Transmission electron microscopy is a powerful imaging technique that uses a focused electron beam to examine the ultrastructure of materials at the nanoscale [50]. When studying cobalt phthalocyanine, TEM can reveal its internal morphology, crystal structure, and elemental distribution [51,52].

f) Raman Spectroscopy

Raman spectroscopy of cobalt phthalocyanine (CoPc) is a powerful analytical technique used to investigate the vibrational and structural properties of a compound [47]. In Raman spectroscopy, a sample is illuminated by a laser source, and the scattered light is examined for wavelength changes that reveal details about the molecular vibrations and structural properties. Applying this approach to CoPc exposes important details about its chemical composition, such as the vibrational modes of the phthalocyanine ring, cobalt-carbon bonds, and other structural elements. [48,49]

g) BET Isotherm

BET isotherms are graphical representations of the amount of gas adsorbed by a solid as a function of gas pressure at a constant temperature. The isotherm can be used to calculate the specific surface area of a material [58]. The Brunauer-Emmett-Teller (BET) hypothesis describes the physical adsorption of gas molecules on solid surfaces. In contrast to the Langmuir theory, which postulates the creation of a single layer of adsorbate on the adsorbent, this model of adsorption involves many layers.

h) Electrochemical Surface Area

The electrochemical surface area (ECSA) is a term used in electrochemistry to refer to the real surface area of an electrode that is accessible to electrolyte ions for electrochemical reactions [59]. It is important because an electrode's geometric surface area may not be entirely functional for the desired reaction. ECSA is higher for electrodes with rough, porous, or nanostructured surfaces than the geometric surface area.

$$\text{Electrochemical surface area} = \frac{\text{Capacitance (F)}}{\text{Specific capacitance (F}cm^{-2}\text{)}}$$

Chapter 3

RESULTS AND DISCUSSION

Cobalt phthalocyanine (CoPc) needs to be properly analysed in order to be used in a variety of applications and to comprehend its characteristics. Researchers employ a range of characterization techniques to analyze CoPc thoroughly. Its electronic structure and vibrational modes can be understood by spectroscopic methods including UV-Vis and infrared spectroscopy. Both X-ray diffraction and electron microscopy can provide details on the morphology and crystalline structure of a substance. As was already said, Raman spectroscopy aids in the identification of vibrational modes and structural changes. As a part of material characterization, X-ray diffraction, UV Vis, and FTIR are performed as primary analysis, and for structural analysis Raman and TEM.

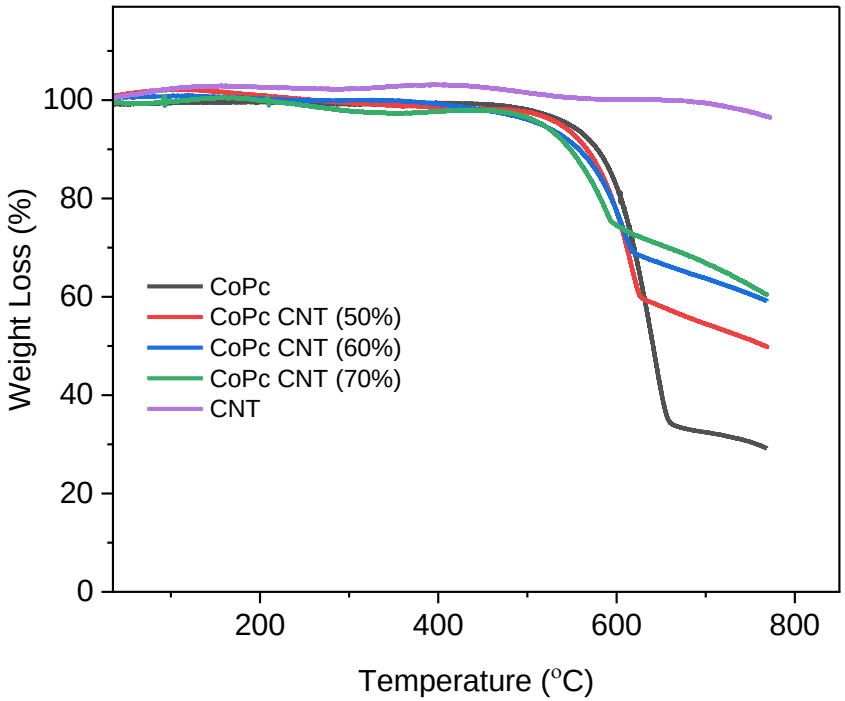

Figure 3.1: Thermogravimetric analysis of pristine CoPc and its composites.

Pyrolysis temperature was selected by analyzing the degradation temperature of composites using Thermal Gravimetric plot given in figure 3.1. Figure 3.1 shows the thermal decay of materials as a rise in temperature. There is a significant weight loss

at around 650℃ for all three materials and the carbonization is almost complete at around 700℃. Therefore, a temperature of 700℃ was chosen for pyrolysis. There is a significant weight loss at around 650℃ for all three materials and the carbonization is almost complete at around 700℃. Therefore, a temperature of 700℃ was chosen for pyrolysis.

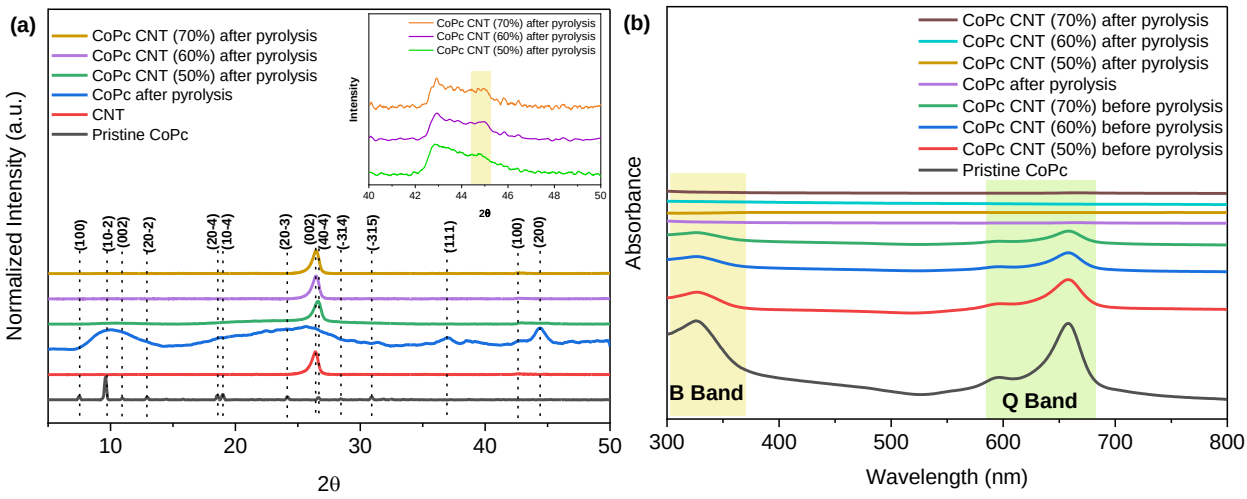

Figure 3.2: (a) X-ray Diffraction of pristine CoPc, CNT and pyrolyzed composites. (b) UV-Vis spectrum of pristine CoPc, and composites before after pyrolysis.

From figure 3.2(a), pristine CoPc shows many sharp peaks from 7.1 to 33.2° with the 2θ corresponding to 7.1° and 9.2° peaks being typical of CoPc crystal. After pyrolysis, a broad peak is observed between 18° and 30°, this is due to the presence of amorphous carbon formation. A sharp peak at 2θ = 44.2° corresponding to cobalt oxide particles [5] is observed on 700°C pyrolyzed CoPc, which means the decomposition or structural changes of the molecule at high temperature. After pyrolysis of materials, there is no peak corresponding to pristine cobalt phthalocyanine and there is only a sharp peak around 26° representing CNT [45]. The absence of pristine CoPc peaks refers to the structural changes in the molecule.

UV-Vis spectra given in the figure 3.2(b) of CoPc show both Q band and B band which corresponds to the electronic transition to a higher energy level (π to π*) or interaction between the metal ion and macrocyclic phthalocyanine ring. But after pyrolysis, these two transitions are absent which refers to the loss of this transition or some structural changes. For Cobalt phthalocyanine, there are 3 significant peaks. But after pyrolyzed CoPc, there are absence significant peaks. Figure 3.2(b) shows some structural

changes that occurred after pyrolysis that caused the absence of electronic transitions in the visible range.

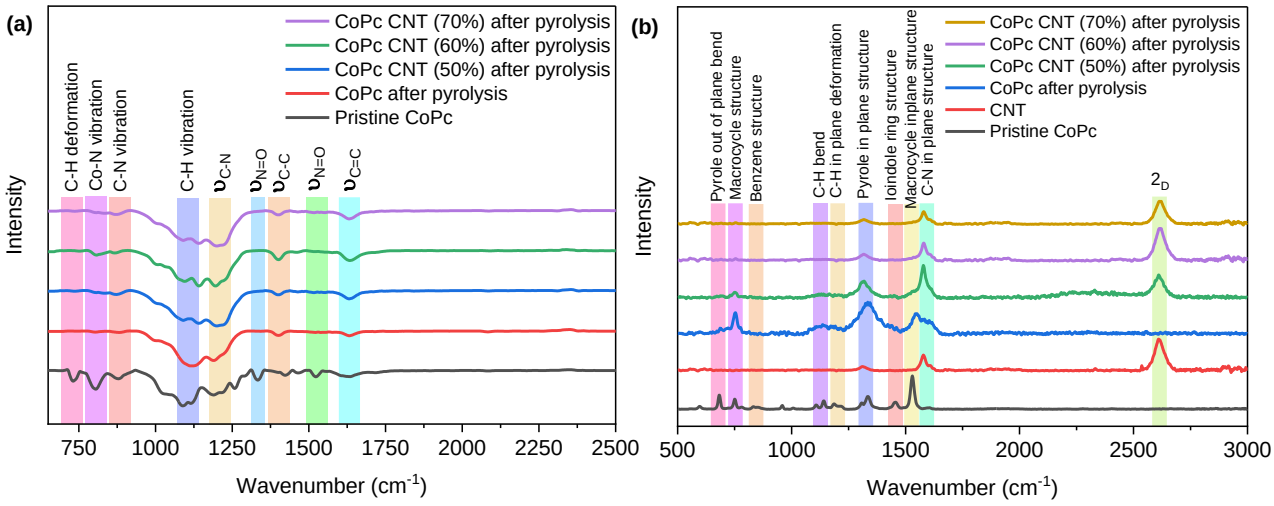

Figure 3.3: (a) FTIR spectra of pristine CoPc, and composites before and after pyrolysis. (b) Raman spectra of pristine CoPc, and composites before and after pyrolysis.

Pristine cobalt phthalocyanine molecule, multiple vibrations are present like C-N, C-H, Co-N, C=C, C=N, etc [39]. But in after pyrolyzed material, these vibrations are less intense. This may be due to some structural changes during the process. Since there is a presence of carbon material, we can compare the I_D/I_G values using Raman spectroscopy in the range of 500 cm^{-1} to 3000 cm^{-1}.[51] I_D/I_G increases means defect is also increasing. Due to the presence of CNT, this ratio will be more than the pristine's ratio.

Table 4: I_D/I_G ratio extracted from the Raman spectra.

Material	I_D/I_G ratio
MWCNT	0.2686
CoPc CNT (50%) After Pyrolysis	0.5342
CoPc CNT (60%) After Pyrolysis	0.3835
CoPc CNT (70%) After Pyrolysis	0.3487

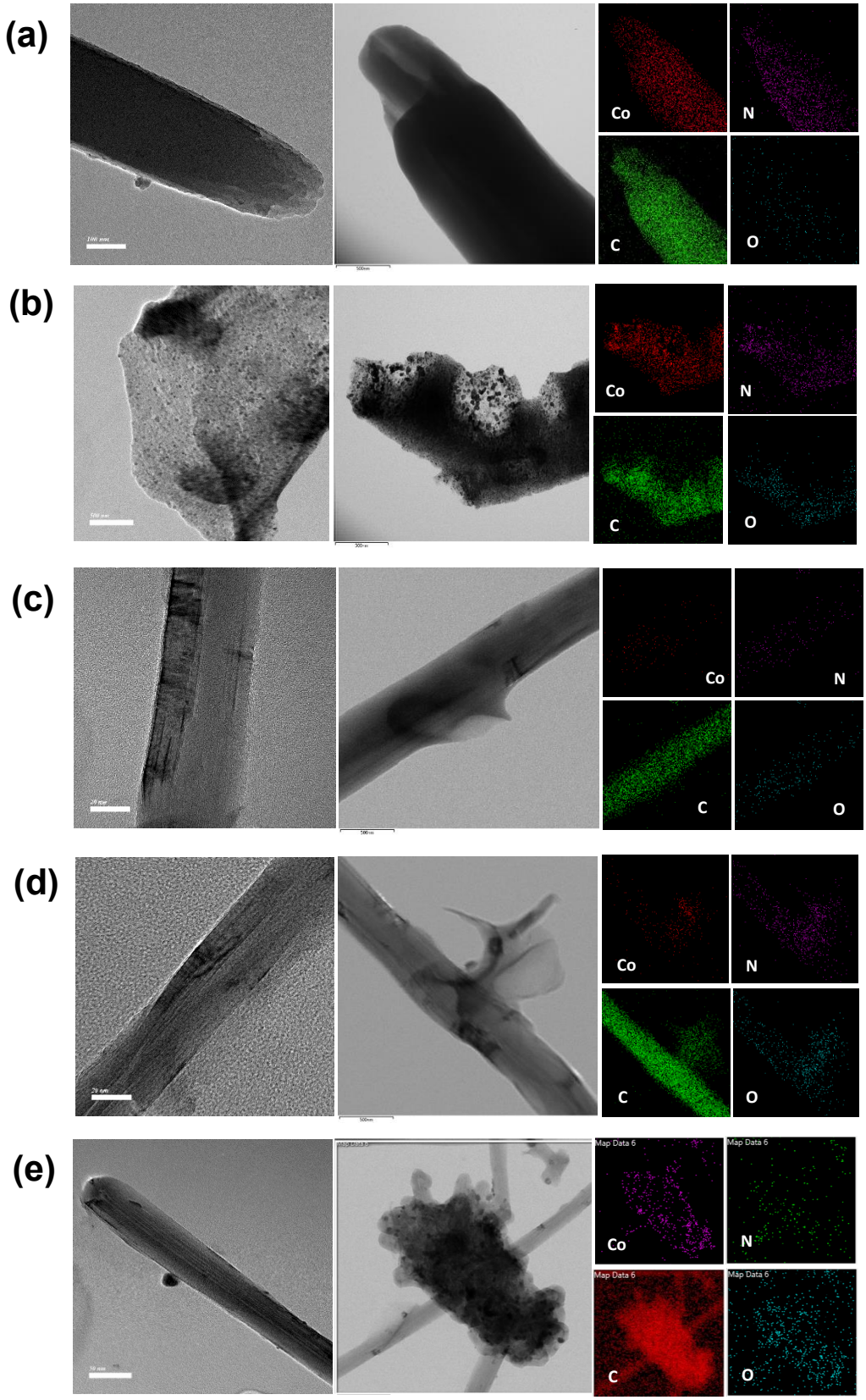

Figure 3.4: TEM and EDX of (a) pristine CoPc (b) CoPc after pyrolysis. (c) CoPc CNT (50%) after pyrolysis, (d) CoPc CNT (60%) after pyrolysis and (e) CoPc CNT (70%) after pyrolysis.

With the help of TEM, we can see the two-dimensional detailed structure of all materials. Here in figure 3.4, we can see parallel lines in the TEM image at higher magnification which implies the presence of crystalline structure and from this we can find the interplanar distance as well. Elemental mapping is also very useful for understanding the elemental composition of the material. The CoPc exhibited a large rectangular sheets like morphology which is absent in after pyrolyzed structure.

Electrochemical characterizations were carried out in Biologic instrument and we have performed various electrochemical techniques like cyclic voltammetry, linear sweep voltammetry and electrochemical impedance spectroscopy for checking the electrochemical activity of all the materials. These techniques help us to understand which is more active and stable for the nitrate removal from the solution. These were carried out in same set of experimental conditions. Linear sweep voltammetry was carried out in 20mM $HClO_4$ in the same potential window of 0 V to -0.9 V (v/s Ag/AgCl/Cl^-). $HClO_4$ is stable in this potential range and also it provides acidic condition [55]. As a nitrate source we can use KNO_3 or $NaNO_3$ because both have similar ionic mobility, we used Sodium nitrate ($NaNO_3$) as a source of nitrate.

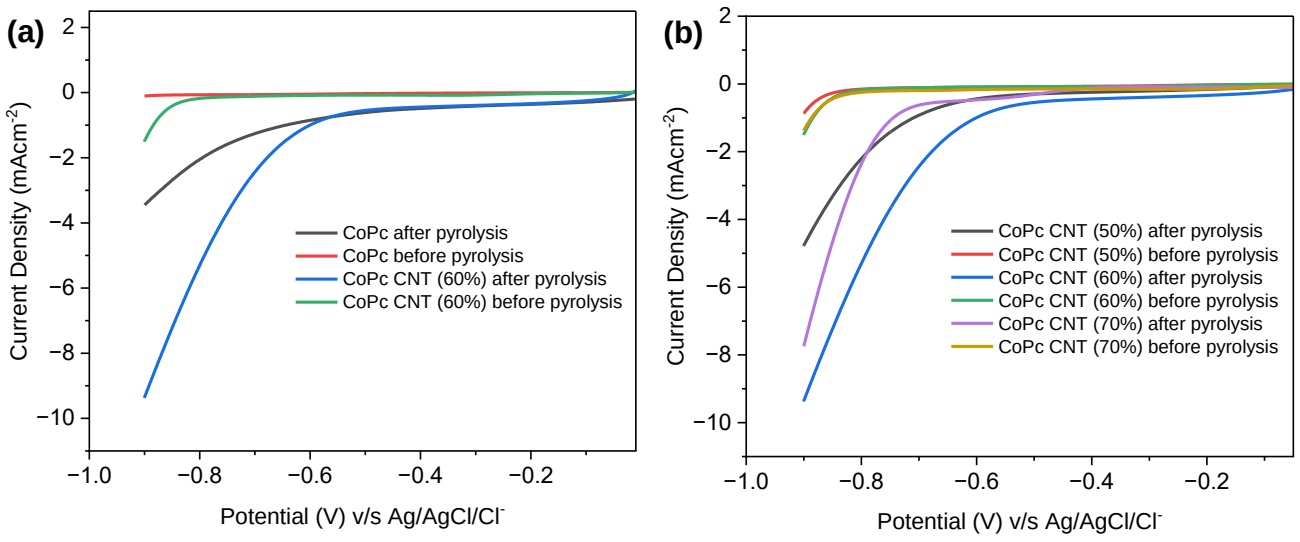

Figure 3.5: Linear sweep voltammetry of (a) pristine CoPc, CoPc after pyrolysis and CoPc CNT (60%) after pyrolysis. Linear sweep voltammetry of (b) CoPc CNT (50%) before and after pyrolysis, CoPc CNT (60%) before and after pyrolysis, and CoPc CNT (70%) before and after pyrolysis.

At higher potential Hydrogen evolution reaction (HER) will dominate this reaction will mask our desired reaction. Therefore, our potential window is restricted to -0.9 V (v/s Ag/AgCl/Cl^-). From the LSV given in figure 3.5(a) and 3.5(b), we can see change in current density is greater in CoPc CNT (60%) after pyrolyzed material. This is an indication of the electrochemical activity of the materials towards nitrate reduction. These LSV experiments were performed in a single compartment 3-electrode cell setup consisting of glassy carbon as the working electrode, Pt disc as the counter electrode, and Ag/AgCl as the reference electrode. From this LSV it is clear that after pyrolyzed materials are showing better electrochemical activity than pristine CoPc and respective composites.

Tafel slopes were calculated to determine the kinetics of these after pyrolyzed materials towards nitrate reduction. It shows how efficiently an electrode can produce current with respect to changes in applied potential. For this, glassy carbon electrode was drop casted with materials and dipped in a 10 mM nitrate solution, and an LSV was performed at 0.5 mV/s scan rate. A linear graph is drawn between the overpotential (η) v/s Log of current density.

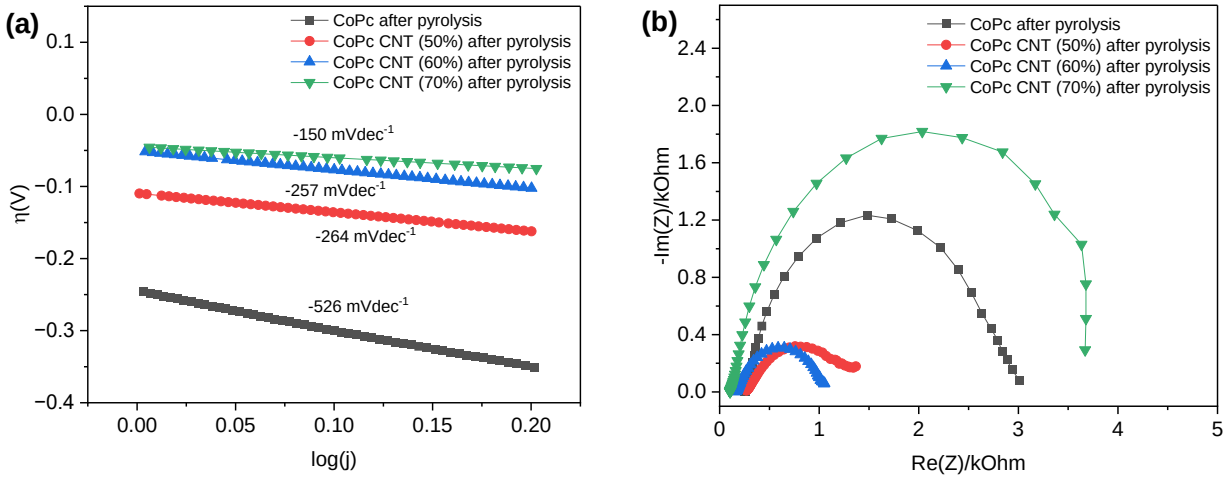

Figure 3.6: (a) Tafel plots of pyrolyzed CoPc composites. (b) Nyquist plots of pyrolyzed CoPc composites.

From figure 3.6(a), we can see tafel slope is least for CoPc CNT (70%) after pyrolyzed material, which means it has the least activation energy required for the reaction to occur. Electrochemical impedance spectroscopic analysis was carried out to determine the solution resistance and charge passed during the reaction. From Nyquist plot given in figure 3.6(b), we can clearly see composites have less charge

transfer resistance compared to pyrolyzed pristine CoPc. And among the pyrolyzed composites CoPc CNT (60%) has least resistance.

For the product analysis, the two-compartment cell was used to get more product and gas diffusion layer (GDL) electrode was used as working electrode. 10 mg of CoPc CNT (60%) after pyrolyzed material was made into an ink by adding 1 ml IPA and 20 µl Nafion resin as binder. After thorough sonication, this ink was uniformly coated in the electrode coving 4 cm^2 area. As this two-compartment cell is an enlarged version of small cell, same concentration nitrate solution as used in both sides with Pt mesh as counter electrode in one side and reference & working electrode in other compartment. Figure 3.7 shows the model of two compartment setup. Constant stirring and Argon purging are required to prevent Oxygen reduction reaction and Nitrogen reduction reaction which are abundant in the atmospheric air. This nitrate reduction to ammonia is a multi-step reaction with multiple intermediates can be formed during the reaction. A parasitic Hydrogen evolution reaction will also happen as we are using acidic $HClO_4$ solution with nitrate. Initially we started with small concentration of nitrate which is 10 mM in 20 mM $HClO_4$ solution.

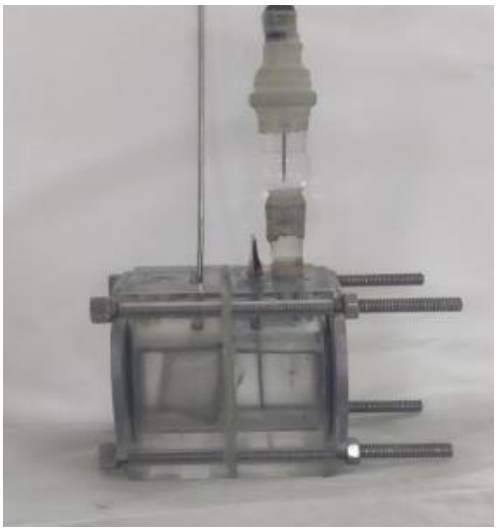

Figure 3.7: Photograph of two compartment cell used for ammonia synthesis.

The product solution was analyzed using NMR and UV-Vis techniques. Nitrate concentration before and after the reaction was calculated using the UV-Vis absorption method in which 100 µL of nitrate solution was diluted to 5 mL and 100 µL 1 M HCl and 10 µL 0.8 wt% sulfamic acid. Different concentrations of nitrate solution were made and absorbance was recorded. Absorbance was measured from 300 nm to 200 nm and a calibration plot was made with absorbance at 220 nm v/s concentration of

nitrate. Figure 3.8(a) shows the UV-Vis spectra of nitrate at different concentrations. A slope was evaluated from the linear fitting given in figure 3.8(b) and with the help of this slope we can easily find out the unknown concentration of nitrate in the solution.

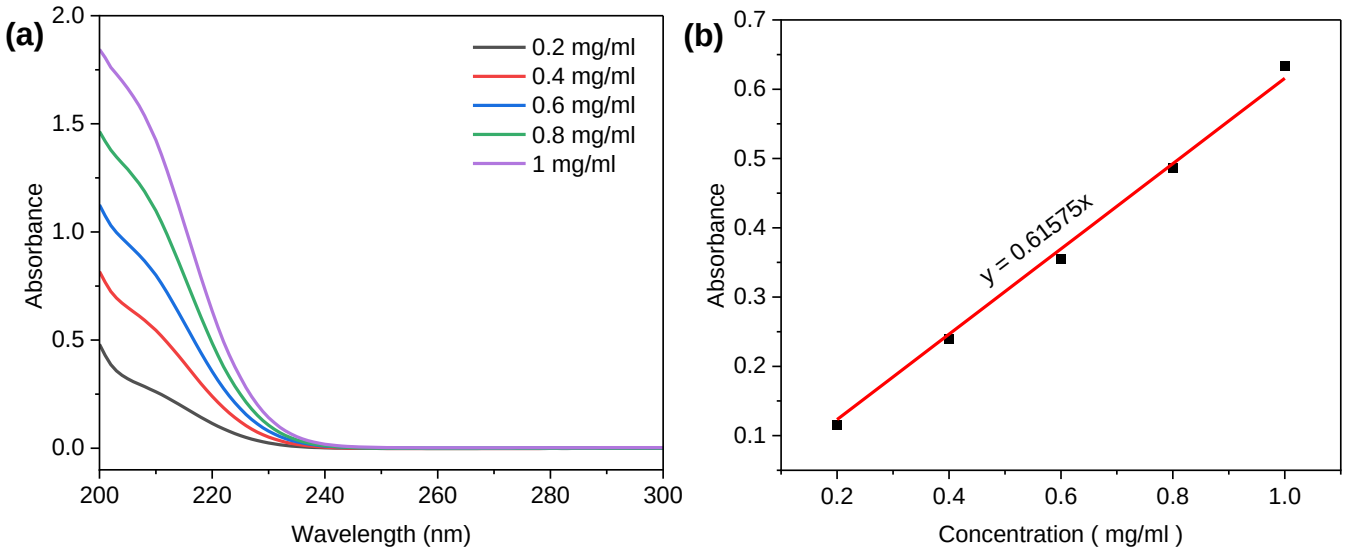

Figure 3.8: (a) UV-Vis spectra of nitrate at different concentrations and (b) the calibration curve for nitrate.

As ammonia is our desired product and this ammonia is found in the product solution as highly water-soluble ammonium ion (NH_4^+) we cannot detect ammonia with the help of mass spectrometry. Quantification of Ammonia was performed with the help of two techniques, one is NMR method and the other one is UV method. In NMR method, different concentrations of ammonium chloride solutions were made and 0.5 ml of the solution was pipetted out into the NMR tube. In the ammonium solution, 50 µl of 0.5 M H_2SO_4, 50 µl of DMSO-d_6, and 10 µl of 12.5 mM maleic acid were added and these solutions were sonicated for 30 mins. There are three peaks corresponding to ammonium ion between 6.8 and 7.2 ppm given in figure 3.9(a). Here we used Maleic as an internal reference standard. For the calibration of ammonium ion in the solution, we took the ratio of the peak integral intensity of all 3 ammonium ion peaks and maleic acid peak. A plot was drawn between intensity ratio v/s concentration of ammonium chloride given in figure 3.9(b). From this graph we got a slope and with the help of this slope we can determine concentration of unknown solution means product solution. ^{1}H NMR was performed in 400 MHz instrument.

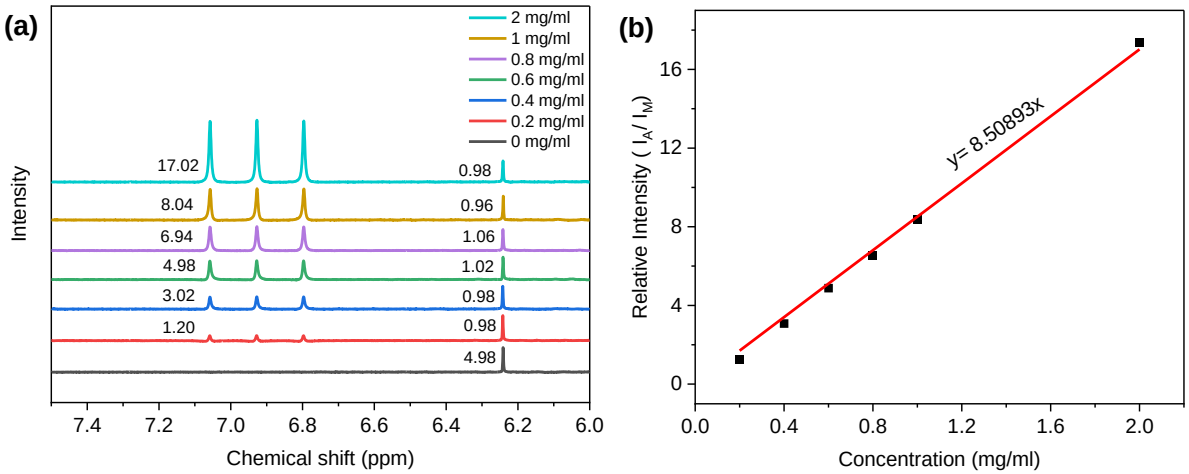

Figure 3.9: (a) ^{1}H NMR spectra of ammonium ion at different concentrations and (b) calibration curve for ammonium ion.

UV-Vis calibration of ammonia was performed using Indophenol method. Different concentrations of ammonium solutions were made and UV-Vis absorption of the corresponding solution was measured in between 500-800 nm given in figure 3.10(a). 400 µl of Phenol: ethanol (9:1) was added to diluted solution of ammonium chloride. Following to this, 400 µl of 0.5 wt% sodium nitroprusside and finally 1ml of a solution containing trisodium citrate, sodium hydroxide, and sodium hypochlorite were added. Depending on the concentration of ammonium, the solution will form dark coloured solution shown in figure 3.10(c). A calibration curve was plotted between absorbance at 640 nm and concentration of ammonium. From this linear graph given in figure 3.10(b), we will get a slope, which we can use it for determining the unknown concentration in the product solution.

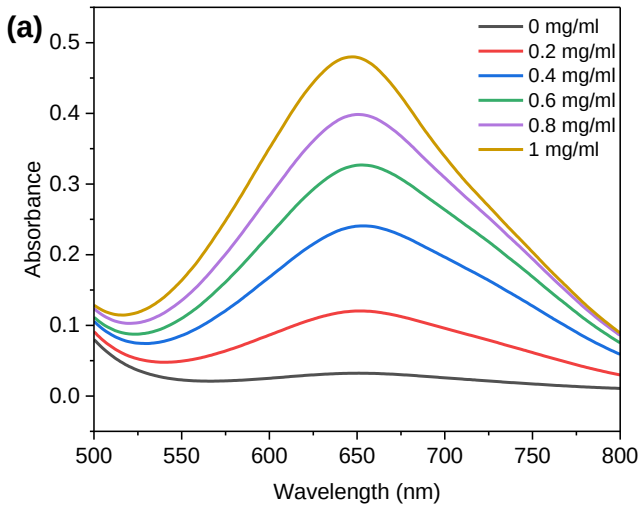

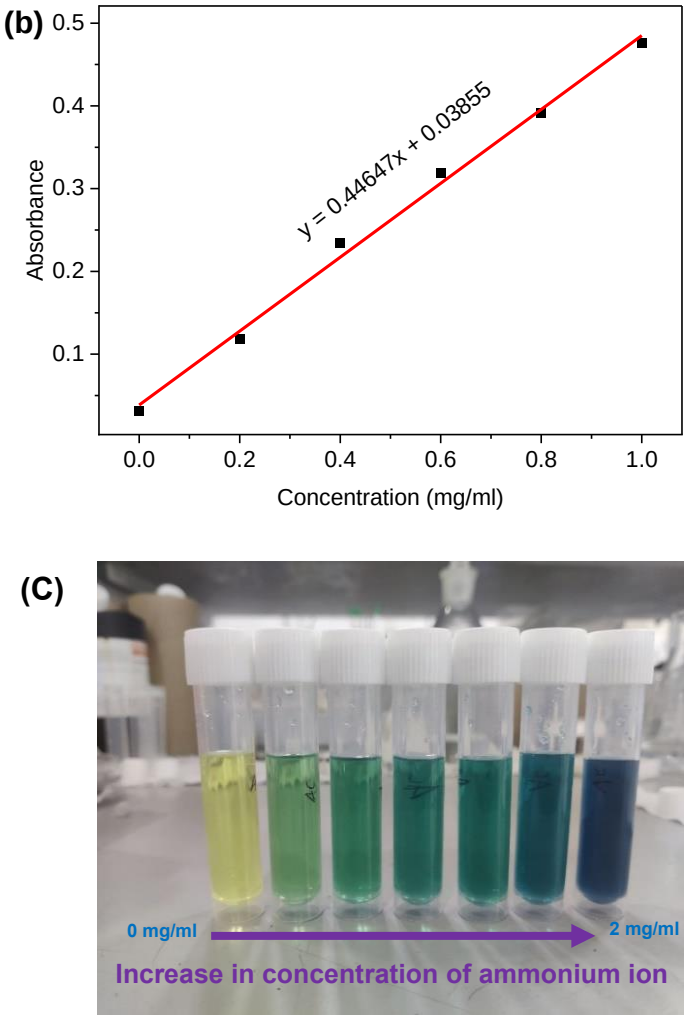

Figure 3.10: (a) UV-Vis spectra of ammonium ion at different concentrations. (b) Calibration curve for ammonium ion at different concentrations. (c) Photographs of ammonia solutions at different concentrations with indophenol blue.

Quantification of nitrite in the product solution also requires a calibration curve. For calibration, we made different concentrations of nitrite solution and 100 µl of standard solution diluted to 5 ml and 0.1 ml of colouring solution was added. The colouring solution includes 0.2 g naphthyl ethylenediamine dihydrochloride, and 4 g P-amino-benzene sulfonamide added in to a mixture of 50ml distilled water and 10 ml concentrated phosphoric acid. UV-Vis absorbance was measured between 450 nm and 650 nm given in figure 3.11(a). A calibration plot was also made using absorbance at 640 nm and concentration of nitrite (figure 3.11(b)). As concentration of nitrite increases, the colour intensity also increases which is shown in figure 3.11(c).

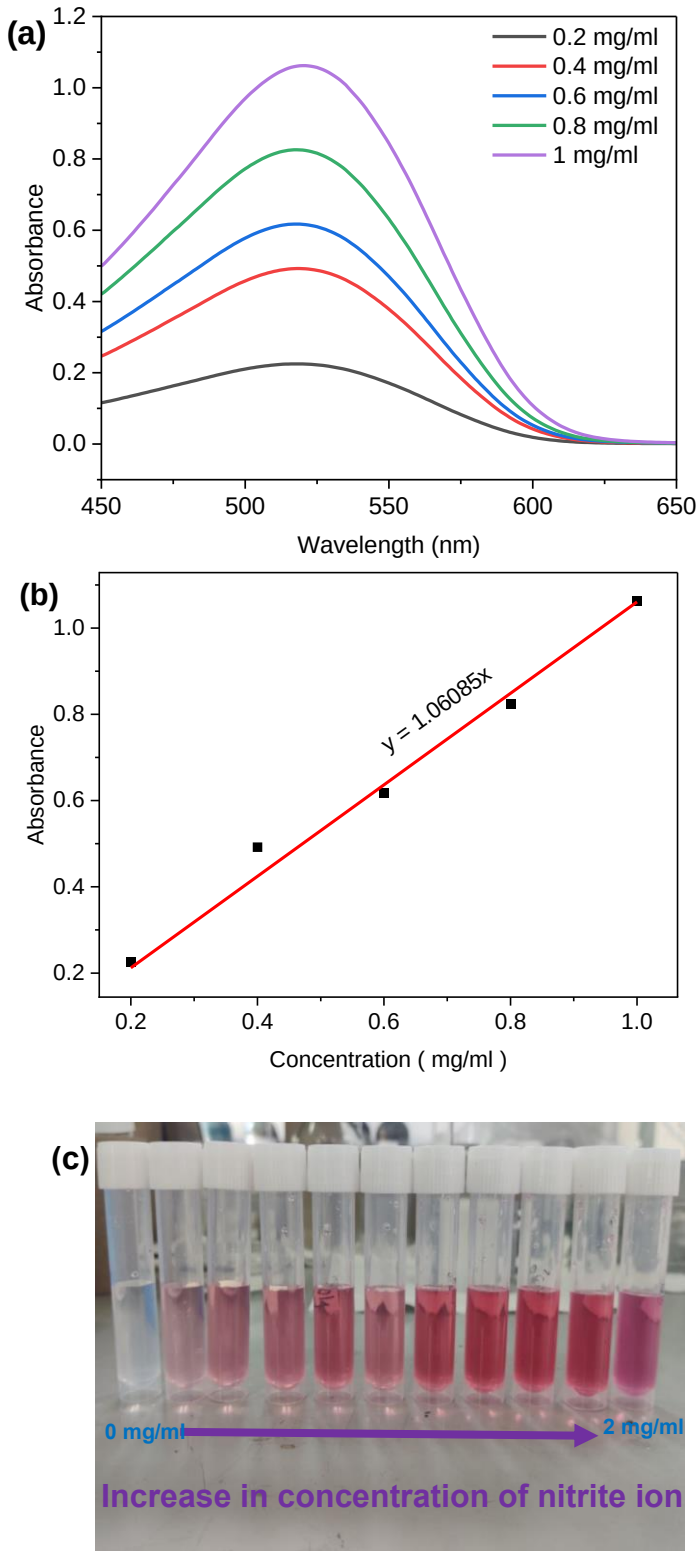

Figure 3.11: (a) UV-Vis spectra of nitrite at different concentrations. (b) Calibration curve of nitrite at different concentrations. (c) Photographs of nitrite solutions at different concentrations with naphthyl ethylenediamine dihydrochloride, and p-amino-benzene sulfonamide.

Since nitrate reduction to ammonia is a multistep reaction, there are possibility of 4 intermediates including NO, NO_2, N_2O, and N_2H_4. Among four, two are in gaseous state therefore we can determine the concentration with the help of an in-situ electrochemical mass spectrometer.

We performed in-situ electrochemical mass spectrometry by applying -30 mA current at working electrode (given in figure 3.12) to determine the presence of H_2 formed as a result of parasitic reaction (HER) and other intermediate gases like NO, N_2O. From figure 3.12 we can see that as our reaction starts, the hydrogen evolution is happening simultaneously. Amount of NO and N_2O are very less or negligible. From this graph we can see the presence of hydrogen qualitatively.

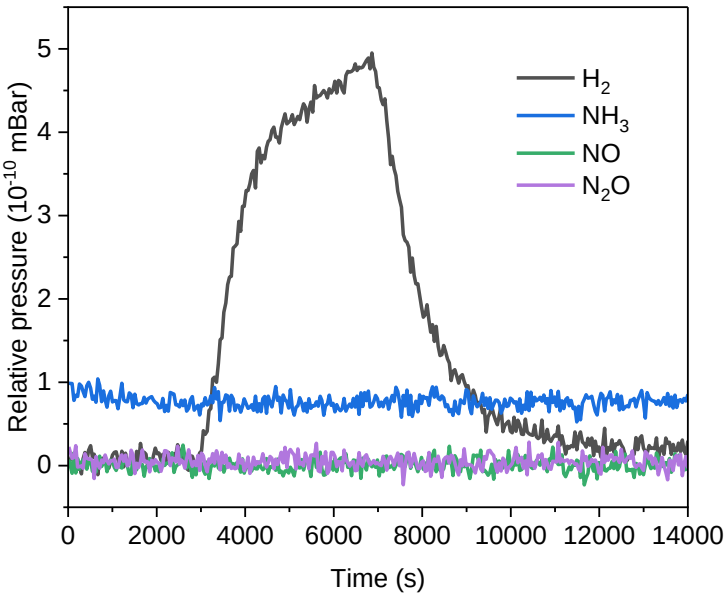

Figure 3.12: In-situ electrochemical mass spectrometry analysis during nitrate reduction showing the presence of hydrogen evolution.

As a part of product analysis, we started with 2 hr chronoamperometry with less concentration of nitrate like 10 mM at different potentials. From this, we came to know that potential from -0.7 V to -1 V (v/s Ag/AgCl/Cl^-) shows more nitrate conversion. The Chronoamperometry profile is shown in Figure 3.13(a) and the product solutions were subjected to NMR and UV-Vis for analyzing Ammonium ions (figure 3.13(b)) and remaining nitrate (figure 3.13(c)) respectively. Yield rate and faradaic efficiency was calculated and plotted with respect to potential in Figure 3.13(d).

$$Faradaic\ Efficiency\ = \frac{Ammonium\ formed\ in\ moles}{Charge\ passed\ in\ moles}\ X\ 100$$

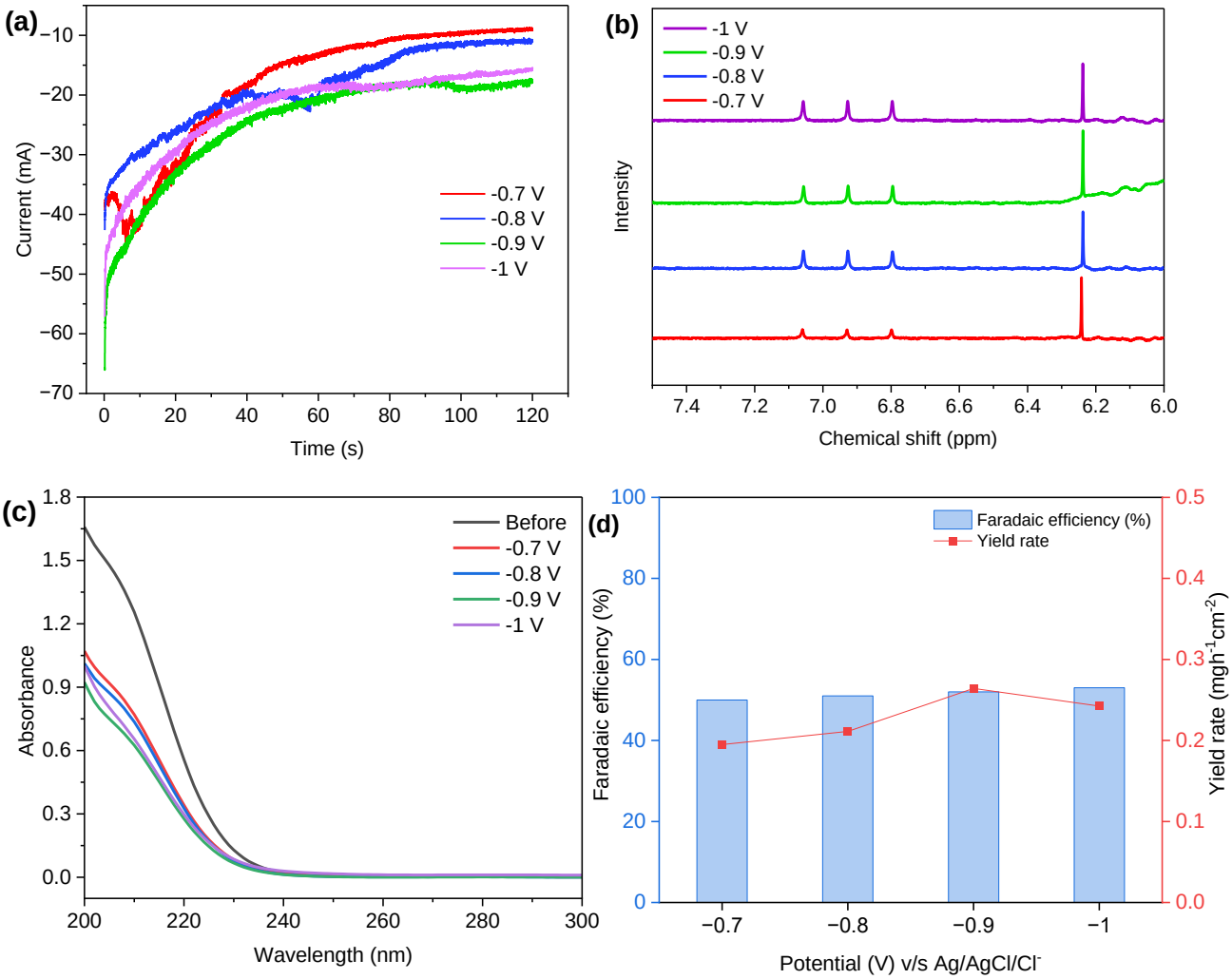

Figure 3.13: (a) Chronoamperometry traces at different potentials for 2 h. (b) ^{1}H NMR spectra demonstrating ammonium ion formation. (c) UV-Vis spectra of nitrate before and after reaction. (d) Yield rate and Faradaic efficiency at different potentials.

After 2hr chronoamperometry experiment we can only see maximum of 52% nitrate removal from the solution. To increase the nitrate removal, we tried CA at different time periods and 20 hr chrono is giving maximum conversion rate of 88%. As the charge passed in 20 hr CA is also much more, our product Faradaic efficiency is reduced significantly.

$$Yield\ rate = \frac{Amount\ of\ ammonium\ formed(mg)}{Total\ time(h) * Area(cm^2)}$$

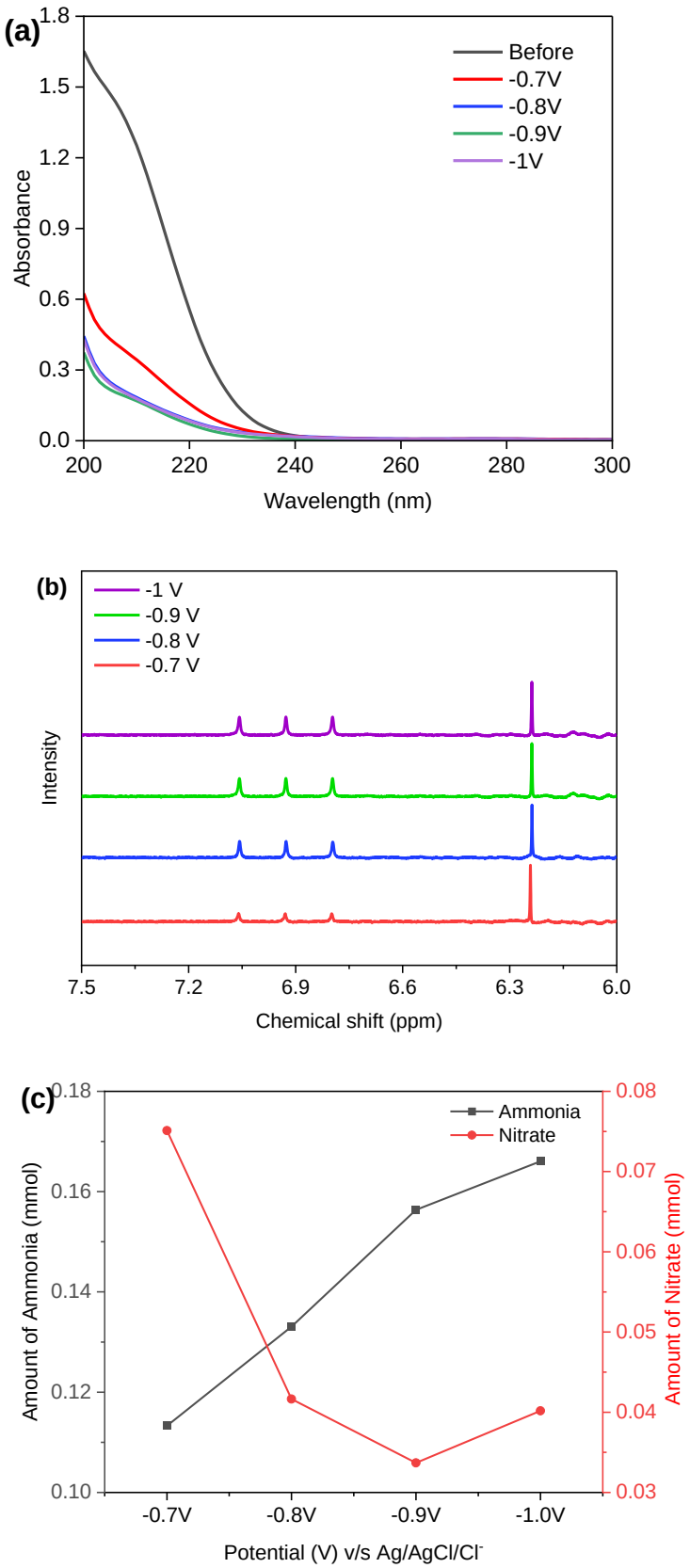

Figure 3.14: (a) UV-Vis spectra of nitrate before and after reaction for 20 h at different potentials. (b) ^{1}H NMR of ammonium ion in the product solution at different potentials. (c) Quantification of ammonium and nitrate in the solution after the reaction.

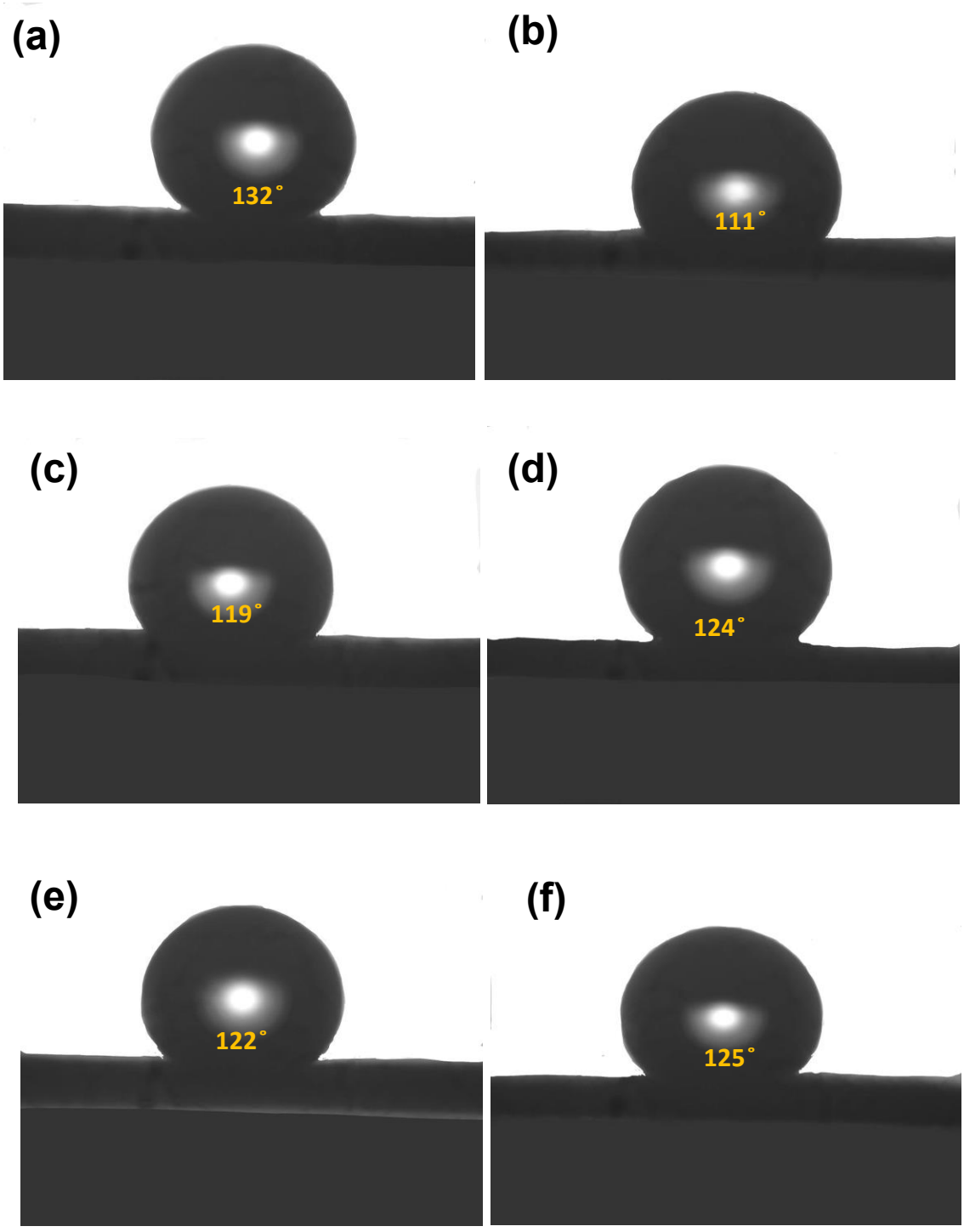

Figure 3.15: Contact angle measurements of (a) MWCNT, (b) pristine CoPc, (c) CoPc after pyrolysis (d) CoPc CNT (50%) after pyrolysis (e) CoPc CNT (60%) after pyrolysis and (f) CoPc CNT (70%) after pyrolysis.

To check the role of surface contact, contact angle measurement study were performed by drop-casting water to the evenly coated surface of materials. Materials were coated in GDL and the angle was measured between the droplet and the surface

of the material. All pyrolyzed composites, CoPc CNT composite materials has fall in the similar range of contact angle, which means compared to CoPc this material has more contact with solution. Figure 3.15 shows contact angle measured. All materials have contact angle greater than 90˚, which means all 6 are hydrophobic in nature. Inorder to use the materials in aqueous system, we dipped the material coated GDL in electrolyte for few hours before prior experiment was carried out.

To check the effect of surface area and the porosity of synthesized composites and pristine molecules BET study were performed given in figure 3.16. The amount of gas adsorbed on the material's surface rises in parallel with the relative pressure (p/p_0). This is because weak attractive forces are causing more gas molecules to collide with the surface and bind together (physisorption). In the BET isotherm plot (amount adsorbed vs. p/p_0), a plateau is seen at a particular relative pressure range, usually 0.05. This plateau denotes the completion of the gas molecule monolayer synthesis on the surface. This plateau area is used by the BET theory to determine the material's specific surface area. Above the plateau, new gas layers grow on top of the first monolayer due to a subsequent increase in relative pressure. We refer to this as multilayer adsorption. Materials with a large number of pores, particularly micropores (pores smaller than 2 nm), may show a sharper initial rise in adsorption at low relative pressures. The reason for this is because the gas fills these micropores first and preferentially.

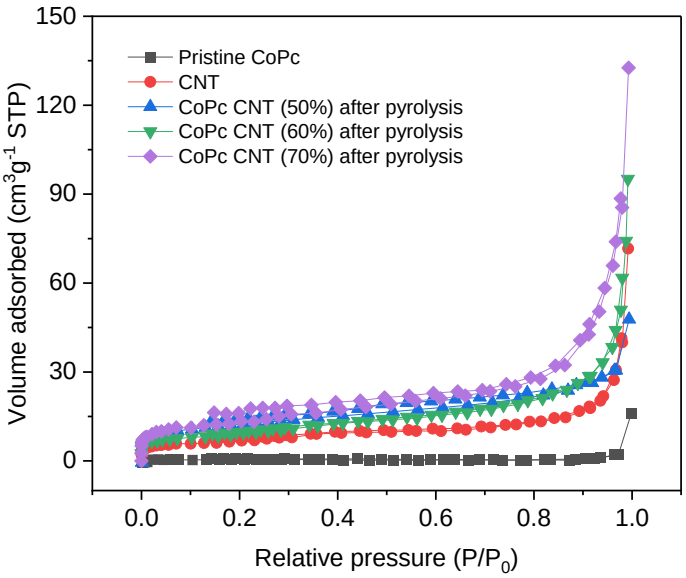

Figure 3.16: BET Nitrogen adsorption desorption isotherm of pristine CoPc, CNT and composites after pyrolysis.

Table 5: Surface areas of CoPc, CNT and the composites before and after pyrolysis.

Materials	**Surface area** ($m^2\ g^{-1}$)	**Pore Volume** ($cm^3\ g^{-1}$)
Pristine CoPc	$1.72*10^{0}$	0.01785
MWCNT	$2.40*10^{+1}$	0.1013
CoPc CNT (50%) after pyrolysis	$4.31*10^{+1}$	0.0697
CoPc CNT (60%) after pyrolysis	$3.28*10^{+1}$	0.1328
CoPc CNT (70%) after pyrolysis	$4.59*10^{+1}$	0.1887

Electrochemical surface area was calculated by drop-casting 20 µl of material ink to the glassy carbon electrode and this electrode was used for taking cyclic voltammogram in the non-faradaic region. In this case we took from +0.6 V to +0.4 V at different scan rates. A plot was made between current and scan rate given in figure 3.17, from this we got the capacitance of the respective material. This capacitance of every material was divided by specific capacitance of glassy carbon which is 0.027 mF cm^{-2} [60] will give the surface area.

ECSA measurement requires specific methodologies for different materials. Methods such as electrochemical impedance spectroscopy (EIS) and cyclic voltammetry are frequently employed. While ECSA concentrates on the electrochemically active region, BET surface area, as determined by gas adsorption, represents the entire surface area. They might not always be related. Perforated or high porosity materials, such as metal oxides and some types of carbon, have more accessible surface area, which causes them to have bigger ECSA. Since nanoparticles have a large surface area to volume ratio, they frequently show substantial ECSA. From the surface area calculation, we can see a significant increase in after pyrolyzed structure than pristine molecule. This may be due to the formation of CoO and Co-N_x nanomaterial formation and graphitic or amorphous carbon which is also contain many pores.

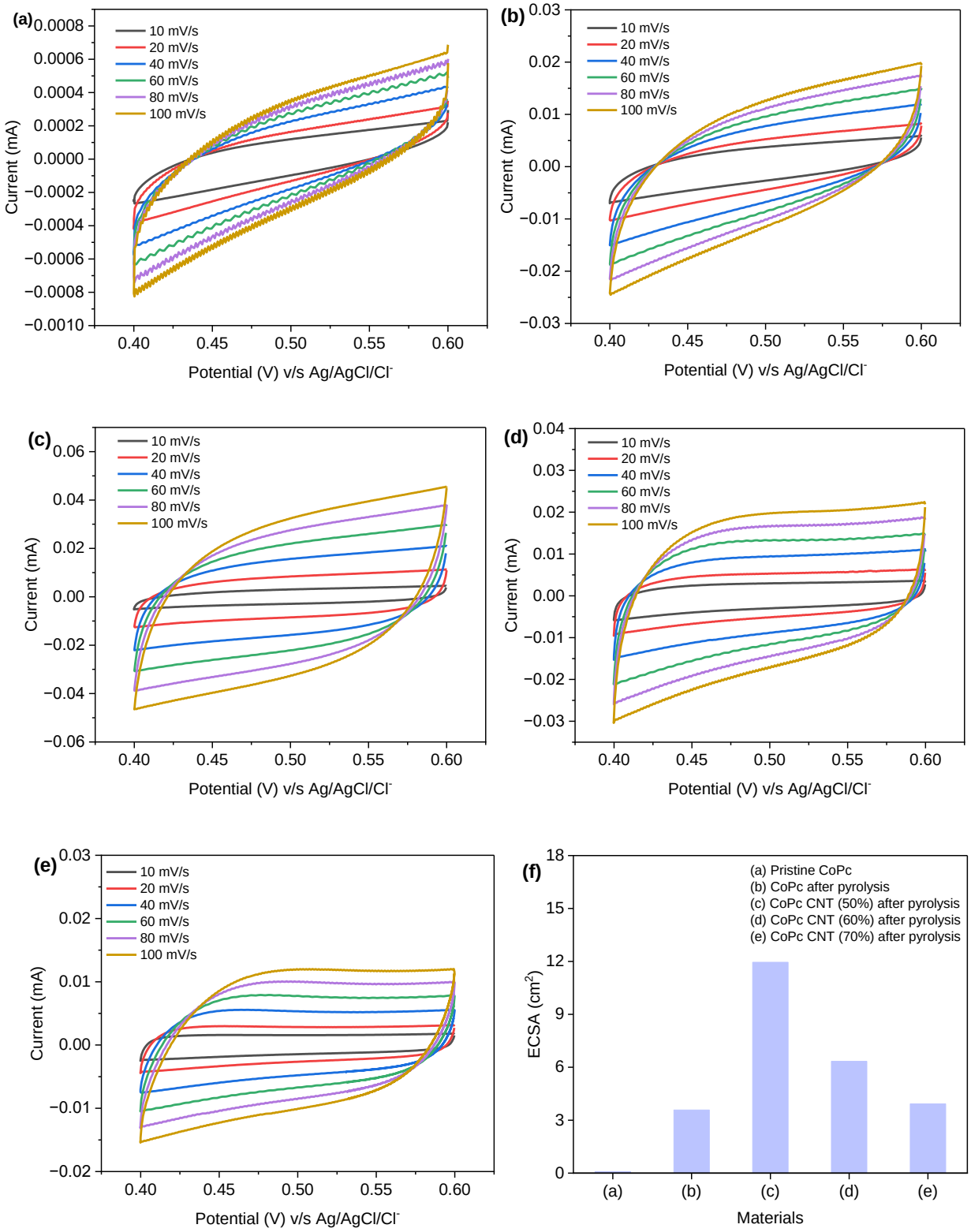

Figure 3.17: Cyclic voltammograms of (a) pristine CoPc, (b) CoPc after pyrolysis, (c) CoPc CNT (50%) after pyrolysis, (d) CoPc CNT (60%) after pyrolysis, (e) CoPc CNT (70%) after pyrolysis and (f) Electrochemical active surface area (ECSA).

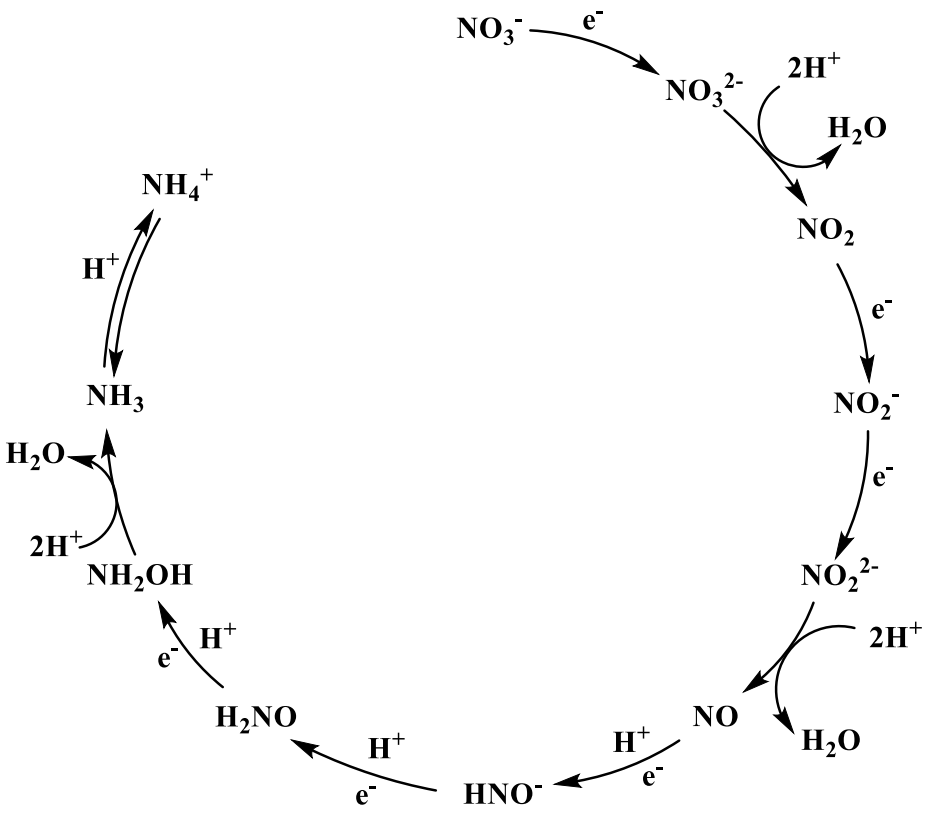

Figure 3.18: Schematic representation of ammonia synthesis during electroreduction of nitrate.

By evaluating the physiochemical and electrochemical characterizations we can clearly see that the activity of after pyrolyzed materials has increased significantly. This is not completely due to the presence of carbon nanotubes but due to the formation of cobalt oxides and Co-Nx sites. Since the carbon nanotubes are not degraded at 700 ℃, this can provide stability to the synthesized cobalt oxide. We proposed a mechanism for electrochemical nitrate reduction using pyrolyzed composites catalyst given in Figure 3.19. Co-N_x and CoO/Co_2O_3 on carbon nanotubes play a crucial role in determining electrochemical activity. Maximum decomposition is happening in the range of 400-600 ˚C and after this temperature CoPc structure decomposes to Co-N_x and carbon. On further heat treatment, metallic Co will form. Since the contact angles given in Figure 3.15 are more than 90° with a similar range, there were no noticeable impacts of the various carbon N and O group concentrations on the electrode surfaces' wettability. This indicates that the electrode's contact with the electrolyte was

hydrophobic, which is explained by the carbon's graphitic nature and its uniform combination with the Nafion binder. Electrochemical surface area data (figure 3.17) shows that pyrolyzed materials have more or less similar electrochemical area compared to pristine CoPc. Therefore, wettability factors or ECSA are not the primary indicators of electrocatalytic disparity for different weight ratios of pyrolyzed materials. The pyrolyzed CoPc-CNT (60%) catalyst results in a notable ammonia yield of nearly 0.26 mg h^{-1} cm^{-2} with a Faradaic efficiency as high as 53% (at -0.9 V vs Ag/AgCl/Cl^-). The notably higher activity of CoPc-CNT (60%) may be due to the better dispersion of Co oxide and Co-Nx sites on the carbon support. An increase in the carbon content (CoPc-CNT (70%)) may decrease the number of catalytic sites that in turn should decrease electrochemical activity. On the other hand, a corresponding decrease in the carbon content (CoPc-CNT (50%)) should affect the well dispersion of the catalytic sites on the carbon support, which should also decrease electrochemical activity. Therefore, the improved performance with varied carbon content is primarily attributed to the uniform distribution of Co-N_x and Co oxide sites on the carbon support.

Based on these experimental observations, Figure 3.18 is proposed for nitrate reduction mechanism which involves a sequential 8 electron transfer mechanism. Figure 3.19 is suggested for the improved activity of the catalysts after pyrolysis towards the nitrate reduction via the enrichment of the carbon support with catalytically active Co-Nx and Co oxide sites.

Perforated materials, such as metal oxides and some types of carbon, have more accessible surface area, which causes them to have bigger ECSA. Since nanoparticles have a large surface area to volume ratio, they frequently show substantial ECSA. From the surface area calculation, we can see a significant increase in after pyrolyzed structure than a pristine molecule. This may be due to the formation of CoO and Co-Nx nanomaterial formation and graphitic or amorphous carbon which also contain many pores.

CoPc CNT (60%) after pyrolysis has uniformly formed material supported on CNT but in CoPc CNT (50%) after pyrolysis material lacking enough CNT support and in CoPc CNT (70%) doesn’t have enough catalytic centre. This is the reason why CoPc CNT (60%) after pyrolyzed material is showing better performance compared to other composites.

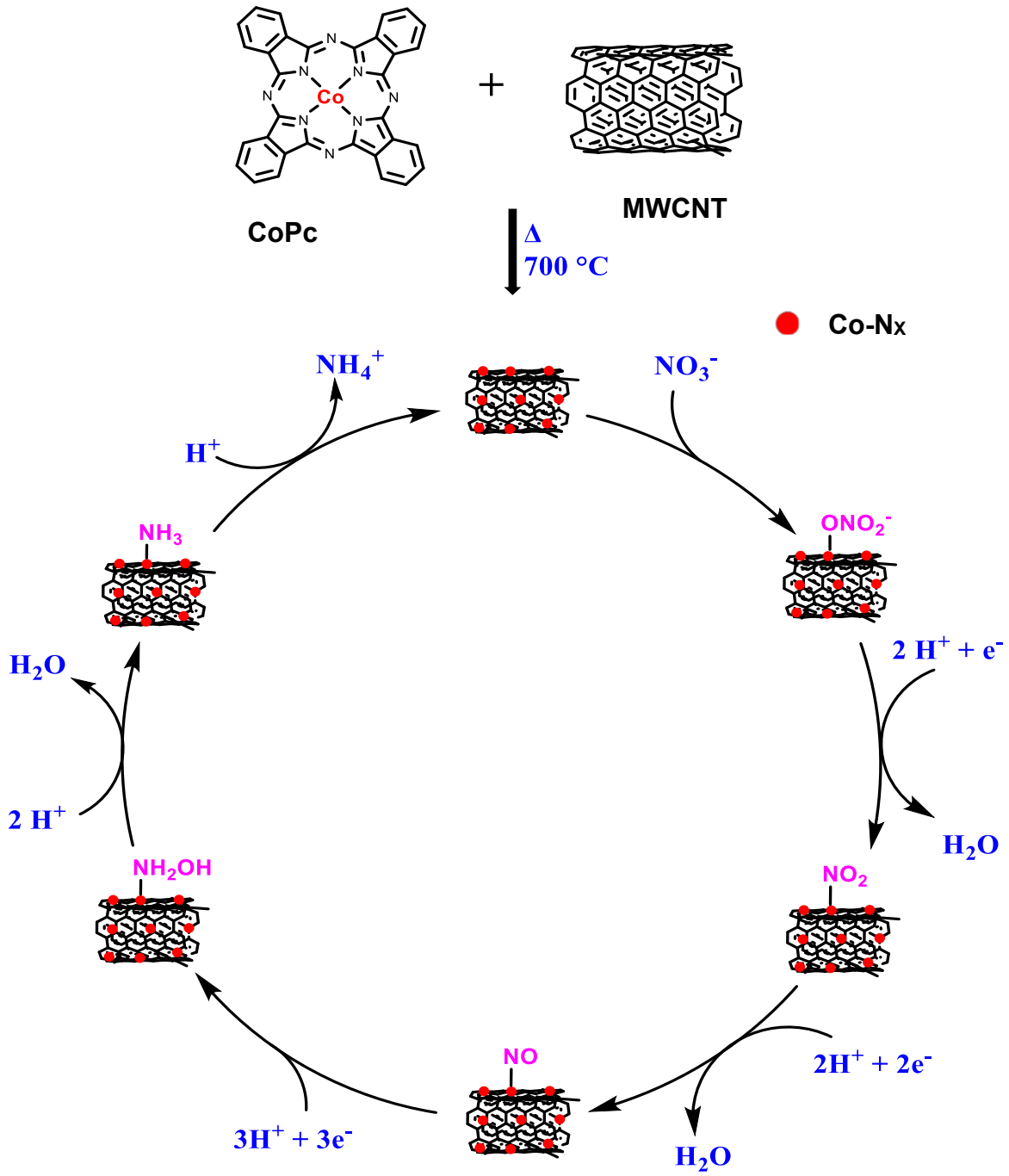

Figure 3.19: Schematic representation of the catalytic cycle describing electrochemical nitrate reduction on pyrolyzed cobalt catalyst.

Chapter 4

CONCLUSION

In this study, CoPc and MWCNT composites were pyrolyzed at 700°C to fabricate a catalyst for nitrate reduction to ammonia. Electrochemical activity has increased drastically after pyrolysis, which makes them suitable candidates for nitrate reduction to ammonia. Electrochemical analysis suggest that pristine CoPc activity is much lower compared to carbon nanotube composites samples indicating the presence of MWCNT helps in facilitating the electron transfer. Various characterization techniques like FTIR, Raman and UV-Vis spectroscopy show that there are structural changes after heat treatment that include the formation of cobalt oxide and Co-Nx sites along with graphitic carbon after pyrolysis. Such metal deposits on MWCNT are believed to have crucial roles in enhancing the performance of pyrolyzed materials. It is observed that CoPc-CNT (60%) after pyrolysis has more activity and stability towards nitrate reduction than CoPc-CNT (50%) and CoPc-CNT (70%). The pyrolyzed CoPc-CNT (60%) catalyst results in a notable ammonia yield of nearly 0.26 mg h^{-1} cm^{-2} with a Faradaic efficiency of nearly 53% at -0.9 V vs Ag/AgCl/Cl^-. The notably higher activity of CoPc-CNT (60%) may be due to the better dispersion of Co oxide and Co-Nx sites on the carbon support. An increase in the carbon content (CoPc-CNT (70%)) may decrease the number of catalytic sites. On the other hand, a corresponding decrease in the carbon content (CoPc-CNT (50%)) should affect the well dispersion of the catalytic sites on the carbon support. Therefore, the improved performance with varied carbon content is primarily attributed to the uniform distribution of Co-N_x and Co oxide sites on carbon support.

REFERENCES

1. Karki, G., Bhatta, B., Devkota, N. R., Acharya, R. P., & Kunwar, R. M. (2022, February 11). Climate change adaptation (CCA) research in Nepal: implications for the advancement of adaptation planning. Mitigation and Adaptation Strategies for Global Change, 27(3). https://doi.org/10.1007/s11027-021-09991-0

2.Basics of Climate Change | US EPA. (2023, November 1). US EPA. https://www.epa.gov/climatechange-science/basics-climate-change

3.Ritchie, H., Rosado, P., & Roser, M. (2024, January 5). Fossil fuels. Our World in Data. https://ourworldindata.org/fossil-fuels

4.Facts about the climate emergency. (n.d.). UNEP - UN Environment Programme. https://www.unep.org/facts-about-climate-emergency

5.Water – at the center of the climate crisis | United Nations. (n.d.). United Nations. https://www.un.org/en/climatechange/science/climate-issues/water

6. Part 5 Climate Change Comes to Piedras Gordas — SHI - Sustainable Agriculture Organic Farming for Poverty Alleviation. (2023, October 17). SHI - Sustainable Agriculture Organic Farming for Poverty Alleviation. https://www.sustainableharvest.org/blog/climatechangecomestopiedrasgordas

7. A., & A. (2023, April 11). Climate Change: Its impact on Food and Nutrition security, Mitigation strategies for coming decades. Action Against Hunger. https://actionagainsthunger.in/climate-change-impact-food-nutrition

8. Energy. (n.d.). Forum for the Future. https://www.forumforthefuture.org/Listing/Category/energy

9. What is renewable energy? | United Nations. (n.d.). United Nations. https://www.un.org/en/climatechange/what-is-renewable-energy

10. Hydrogen and renewable energy companies in Scotland. (n.d.). Scottish Development International. https://www.sdi.co.uk/buy-from-scotland/energy-and-low-carbon-companies/hydrogen-companies

11. Alternative Fuels Data Center: How Do Fuel Cell Electric Vehicles Work Using Hydrogen? (n.d.). https://afdc.energy.gov/vehicles/how-do-fuel-cell-electric-cars-work

12. Maka, A. O. M., & Alabid, J. M. (2022, June 1). Solar energy technology and its roles in sustainable development. Clean Energy, 6(3), 476–483. https://doi.org/10.1093/ce/zkac023

13. Charabi, Y., & Abdul-Wahab, S. (2020, August 17). Wind turbine performance analysis for energy cost minimization. Renewables: Wind, Water, and Solar, 7(1). https://doi.org/10.1186/s40807-020-00062-7

14. Hellerschmied, C., Schritter, J., Waldmann, N., Zaduryan, A. B., Rachbauer, L., Scherr, K. E., Andiappan, A., Bauer, S., Pichler, M., & Loibner, A. P. (2024, February 16). Hydrogen storage and geo-methanation in a depleted underground hydrocarbon reservoir. Nature Energy, 9(3), 333–344. https://doi.org/10.1038/s41560-024-01458-1

15. Meda, U. S., Bhat, N., Pandey, A., Subramanya, K., & Lourdu Antony Raj, M. (2023, June). Challenges associated with hydrogen storage systems due to the hydrogen embrittlement of high strength steels. International Journal of Hydrogen Energy, 48(47), 17894–17913. https://doi.org/10.1016/j.ijhydene.2023.01.292

16. Yang, M., Hunger, R., Berrettoni, S., Sprecher, B., & Wang, B. (2023, February 1). A review of hydrogen storage and transport technologies. Clean Energy, 7(1), 190–216. https://doi.org/10.1093/ce/zkad021

17. Dagdougui, H., Sacile, R., Bersani, C., & Ouammi, A. (2018). Hydrogen Logistics: Safety and Risks Issues. Hydrogen Infrastructure for Energy Applications, 127–148. https://doi.org/10.1016/b978-0-12-812036-1.00007-x

18. Farhana, K., Shadate Faisal Mahamude, A., & Kadirgama, K. (2024, February). Comparing hydrogen fuel cost of production from various sources - a competitive analysis. Energy Conversion and Management, 302, 118088. https://doi.org/10.1016/j.enconman.2024.118088

19. Cheddie, D. (2012, October 17). Ammonia as a Hydrogen Source for Fuel Cells: A Review. Hydrogen Energy - Challenges and Perspectives. https://doi.org/10.5772/47759

20. Kubicsek, F., Kozák, R., Turányi, T., Zsély, I. G., Papp, M., Ahmad, A. A., & Hegedűs, F. (2024). Ammonia Production by Microbubbles: A Theoretical Analysis of Achievable Energy Intensity. https://doi.org/10.2139/ssrn.4723811

21. Jadeja, N. B., Banerji, T., Kapley, A., & Kumar, R. (2022, August). Water pollution in India – Current scenario. Water Security, 16, 100119. https://doi.org/10.1016/j.wasec.2022.100119

22. Verma, A., Sharma, A., Kumar, R., & Sharma, P. (2023, November). Nitrate contamination in groundwater and associated health risk assessment for Indo-Gangetic Plain, India. Groundwater for Sustainable Development, 23, 100978. https://doi.org/10.1016/j.gsd.2023.100978

23. (Nitrate and Nitrite in Drinking-water: Background Document for Development of WHO Guidelines for Drinking-water Quality, 2003)

24. Bijay-Singh, & Craswell, E. (2021, March 31). Fertilizers and nitrate pollution of surface and ground water: an increasingly pervasive global problem. SN Applied Sciences, 3(4). https://doi.org/10.1007/s42452-021-04521-8

25. Ward, M., Jones, R., Brender, J., de Kok, T., Weyer, P., Nolan, B., Villanueva, C., & van Breda, S. (2018, July 23). Drinking Water Nitrate and Human Health: An Updated Review. International Journal of Environmental Research and Public Health, 15(7), 1557. https://doi.org/10.3390/ijerph15071557

26. Chen, L., Sagar, R. U. R., Chen, J., Liu, J., Aslam, S., Nosheen, F., Anwar, T., Hussain, N., Hou, X., & Liang, T. (2021, May). Cobalt phthalocyanine as an efficient catalyst for hydrogen evolution reaction. International Journal of Hydrogen Energy, 46(37), 19338–19346. https://doi.org/10.1016/j.ijhydene.2021.03.075

27. Wang, M., Torbensen, K., Salvatore, D., Ren, S., Joulié, D., Dumoulin, F., Mendoza, D., Lassalle-Kaiser, B., Işci, U., Berlinguette, C. P., & Robert, M. (2019, August 9). CO2 electrochemical catalytic reduction with a highly active cobalt phthalocyanine. Nature Communications, 10(1). https://doi.org/10.1038/s41467-019-11542-w

28. Thomas AL. Phthalocyanine Research and Applications. CRC Press; 1990.

29. Lakshmana Naik Ramavathu, Kranthi Kumar Maniam, Keerthiga Gopalram, Chetty R. Effect of pyrolysis temperature on cobalt phthalocyanine supported on carbon nanotubes for oxygen reduction reaction. Journal of Applied Electrochemistry. 2012 Sep 12;42(11):945–51.

30. Chen L, Rizwan, Chen J, Liu J, Aslam S, Farhat Nosheen, et al. Cobalt phthalocyanine as an efficient catalyst for hydrogen evolution reaction. International Journal of Hydrogen Energy. 2021 May 1;46(37):19338–46.

31. K.B. Chandrakala, Giddaerappa Kuntoji, K.R. Venugopala reddy, K.H. Shivaprasad. Investigational undertaking descriptors for reduced graphene oxide-phthalocyanine composite based catalyst for electrochemical oxygen evolution reaction. Journal of Electroanalytical Chemistry. 2022 Aug 1; 919:116558–8.

32. Hamonnet J, Bennington MS, Johannessen B, Hamilton J, Brooksby PA, Brooker S, et al. Influence of Carbon Support on the Pyrolysis of Cobalt Phthalocyanine for the Efficient Electroreduction of CO2. ACS Catalysis. 2022 Nov 14;12(23):14571–81.

33. Zhu I, Getting T. A review of nitrate reduction using inorganic materials. Environmental Technology Reviews. 2012 Nov;1(1):46–58.

34. Serov A, Kwak C. Direct hydrazine fuel cells: A review. Applied Catalysis B: Environmental. 2010 Jul;98(1-2):1–9.

35. Elgrishi, N., Rountree, K. J., McCarthy, B. D., Rountree, E. S., Eisenhart, T. T., & Dempsey, J. L. (2017, November 3). A Practical Beginner's Guide to Cyclic Voltammetry. Journal of Chemical Education, 95(2), 197–206. https://doi.org/10.1021/acs.jchemed.7b00361

36. Morozan A, Campidelli S, Filoramo A, Jousselme B, Palacin S. Catalytic activity of cobalt and iron phthalocyanines or porphyrins supported on different carbon nanotubes towards oxygen reduction reaction. Carbon. 2011 Nov;49(14):4839–47.

37. Sezer, N., & Koç, M. (2019, March). Oxidative acid treatment of carbon nanotubes. Surfaces and Interfaces, 14, 1–8. https://doi.org/10.1016/j.surfin.2018.11.001

38. Lu J, Zhang Y, Gong X, Li L, Pang S, Qian G, et al. High-yield synthesis of ultrathin silicon nanosheets by physical grinding enables robust lithium-ion storage. Chemical Engineering Journal. 2022 Oct 1; 446:137022–2.

39. Bertram Eugene Warren. X-ray diffraction. New York: Dover; 1990.

40. Das R, Hamid S, Ali Md, Ramakrishna S, Yongzhi W. Carbon Nanotubes Characterization by X-ray Powder Diffraction – A Review. Current Nanoscience. 2014 Dec 1;11(1):23–35.

41. Heinz-Helmut Perkampus. UV-VIS Spectroscopy and Its Applications. Berlin, Heidelberg Springer Berlin Heidelberg; 1992.

42. Seoudi R, El-Bahy GS, El Sayed ZA. Ultraviolet and visible spectroscopic studies of phthalocyanine and its complexes thin films. Optical Materials. 2006 Nov;29(2-3):304–12.

43. Ebru Yabaş. New cobalt phthalocyanine–graphene oxide hybrid nanomaterial prepared by strong π–π interactions. Journal of the Australian Ceramic Society. 2021 Oct 4;58(1):63–70.

44. Madejová J. FTIR techniques in clay mineral studies. Vibrational Spectroscopy. 2003 Jan;31(1):1–10.

45. Coats AW, Redfern JP. Thermogravimetric analysis. A review. The Analyst. 1963;88(1053):906.

46. Kumar P, Kumar A, Sreedhar B, Sain B, Ray SS, Jain SL. Cobalt Phthalocyanine Immobilized on Graphene Oxide: An Efficient Visible-Active Catalyst for the Photoreduction of Carbon Dioxide. Chemistry - A European Journal. 2014 Apr 2;20(20):6154–61.

47. Staveley LAK. The characterization of chemical purity : organic compounds. London, England: Butterworth & Co. (Publishers) Ltd; 1971.

48. Subramanian P, Schechter A. Electrochemical Oxygen Reduction Activity of Cobalt-Nitrogen-Carbon Composite Catalyst Prepared by Single Precursor Pyrolysis under Autogenic Pressure. Journal of The Electrochemical Society. 2016;163(5):F428–36.

49. Yan J, Meng H, Yu W, Yuan X, Lin W, Ouyang W, et al. Preparation of nitrogen-doped graphitic carboncages as electrocatalyst for oxygen reduction reaction. Electrochimica Acta. 2014 May 1; 129:196–202.

50. Williams DB, Carter CB. The Transmission Electron Microscope. Transmission Electron Microscopy. 1996;3–17.

51. Karl-Kalev Türk, Ivar Kruusenberg, Mondal J, Protima Rauwel, Kozlova J, Matisen L, et al. Oxygen electroreduction on MN4-macrocycle modified graphene/multi-walled

carbon nanotube composites. Journal of Electroanalytical Chemistry. 2015 Nov 1; 756:69–76.

52. Vallejos-Burgos F, Utsumi S, Hattori Y, Ximena García, Gordon AL, Hirofumi Kanoh, et al. Pyrolyzed phthalocyanines as surrogate carbon catalysts: Initial insights into oxygen-transfer mechanisms. Fuel. 2012 Sep 1; 99:106–17.

53. Ando Y, Zhao X, Shimoyama H, Sakai G, Kaneto K. Physical properties of multiwalled carbon nanotubes. International Journal of Inorganic Materials. 1999 Apr;1(1):77–82.

54. Kimoto K, Toru Asaka, Xia Y, Nagai T, Matsui Y, Ishizuka K. Local crystal structure analysis with several picometer precision using scanning transmission electron microscopy. Ultramicroscopy. 2010 Jun 1;110(7):778–82.

55. Lu X, Song H, Cai J, Lu S. Recent development of electrochemical nitrate reduction to ammonia: A mini review. Electrochemistry Communications. 2021 Aug;129:107094.

56. Maria Yu. Rusanova, Pavla Polášková, Muzikář M, W. Ronald Fawcett. Electrochemical reduction of perchlorate ions on platinum-activated nickel. Electrochimica Acta. 2006 Apr 1;51(15):3097–101.

57. Zhu W, Zhang X, Yao F, Huang R, Chen Y, Chen C, et al. A Hydrazine-Nitrate Flow Battery Catalyzed by a Bimetallic RuCo Precatalyst for Wastewater Purification along with Simultaneous Generation of Ammonia and Electricity. Angewandte Chemie. 2023 Mar 31;62(19).

58. Dollimore, D., Spooner, P., & Turner, A. (1976, March). The bet method of analysis of gas adsorption data and its relevance to the calculation of surface areas. Surface Technology, 4(2), 121–160.

59. Trasatti, S., & Petrii, O. A. (1991, January 1). Real surface area measurements in electrochemistry. Pure and Applied Chemistry, 63(5), 711–734. https://doi.org/10.1351/pac199163050711

60. Wen, Y., Cao, G., Cheng, J., & Yang, Y. (2005). Correlation of Capacitance with the Pore Structure for Nanoporous Glassy Carbon Electrodes. Journal of the Electrochemical Society, 152(9), A1770. https://doi.org/10.1149/1.1984447